Actin-dependent recruitment of Ago2 to the zonula adherens

Mary Catherine Bridges[1], Joyce Nair-Menon[1], Madison E. Davis[1], and Antonis Kourtidis[1]

[1]Department of Regenerative Medicine and Cell Biology, Medical University of South Carolina, 173 Ashley Avenue, Charleston, SC 29425, USA

Correspondence to Antonis Kourtidis: kourtidi@musc.edu

Condensed Title: Junctional recruitment of Ago2 is actin-dependent

Summary: E-cadherin junctions at the zonula adherens recruit the key RNAi component Ago2 through a still unexplored mechanism. The present work shows that junctional recruitment of Ago2 depends on the integrity and tension of the actin cytoskeleton, revealing a mechanosensitive aspect of RNAi.

Abstract
Adherens junctions are cadherin-based structures critical for cellular architecture. E-cadherin junctions in mature epithelial cell monolayers tether to an apical actomyosin ring to form the zonula adherens (ZA). We have previously shown that the adherens junction protein PLEKHA7 associates with and regulates the function of the core RNA interference (RNAi) component Ago2, specifically at the ZA. However, the mechanism mediating Ago2 recruitment to the ZA remained unexplored. Here, we reveal that this ZA-specific recruitment of Ago2 depends on both the structural and tensile integrity of the actomyosin cytoskeleton. We found that depletion of not only PLEKHA7, but also either of three PLEKHA7-interacting, LIM-domain family proteins, namely LMO7, LIMCH1, and PDLIM1, results in disruption of actomyosin organization and tension, as well as loss of Ago2 junctional localization. These results demonstrate that recruitment of Ago2 to the ZA is sensitive to actomyosin perturbations, introducing the idea of a mechanosensitive RNAi machinery, with potential implications in tissue remodeling and in disease.

Introduction

The Adherens Junction (AJ) is a cell-cell adhesive structure essential for epithelial tissue organization and homeostasis (Harris and Tepass, 2010; Meng and Takeichi, 2009; Takeichi, 2014). E-cadherin is the core AJ component that forms extracellular linkages between neighboring cells through calcium-dependent homotypic binding (Takeichi, 1995). Intracellularly, E-cadherin binds to β-catenin and p120 catenin (p120) (Reynolds et al., 1994), with p120 playing a key role in stabilizing cadherin junctions (Thoreson et al., 2000). E-cadherin-based junctions also connect to the actin cytoskeleton through α-catenin (Mege and Ishiyama, 2017), a β-catenin binding partner. In polarized epithelia, these connections mature at an apically localized structure known as the zonula adherens (ZA), which links to a circumferential actin ring (Farquhar and Palade, 1963; Meng and Takeichi, 2009). At the ZA, actin organization is intimately involved in the dynamic interplay between contractile force sensation and junctional stabilization (Kovacs et al., 2002; Kovacs et al., 2011; Leerberg et al., 2014; Priya et al., 2013; Ratheesh and Yap, 2012; Shewan et al., 2005; Smutny et al., 2010; Verma et al., 2012; Yamada and Nelson, 2007).

In addition to their critical architectural role, epithelial AJs mediate numerous signaling pathways directing cell behavior (Daulagala et al., 2019; Kourtidis et al., 2017a; Kourtidis et al., 2013; Mendonsa et al., 2018; Ramirez Moreno and Bulgakova, 2021; Salvi and DeMali, 2018; Yu and Elble, 2016; Yulis et al., 2018). This aspect of AJ biology implicates loss of AJ integrity to the progression of multiple diseases, such as cancer (Daulagala et al., 2019; Kourtidis et al., 2017a; Kourtidis et al., 2013; Mendonsa et al., 2018; Ramirez Moreno and Bulgakova, 2021; Yu and Elble, 2016). Along these lines, we have previously demonstrated that cadherin junctions recruit core complexes of RNA interference (RNAi) machinery, such as the microprocessor and the RNA-induced Silencing Complex (RISC), to locally regulate microRNA (miRNA) processing and function (Kourtidis et al., 2017b; Kourtidis et al., 2015). Loading of miRNAs onto Argonaute 2 (Ago2), the main enzymatic component of the RISC, leads to translational repression or degradation of target mRNAs (Hammond et al., 2001; Huntzinger and Izaurralde, 2011; Liu et al., 2004; Meister et al., 2004). While Ago2 has been shown to be primarily cytoplasmic, its recruitment to distinct subcellular loci is a mechanism by which RISC activity can be regulated (Antoniou et al., 2014; Bose et al., 2020; Bridge et al., 2017; Detzer et al., 2011; Gagnon et al., 2014; James et al., 2010; Leung et al., 2006; Zeng et al., 2008). Our previous work identified recruitment of Ago2 specifically to the ZA of well-differentiated epithelial cells and tissues, but not at basolateral areas of cell-cell contact (Kourtidis et al., 2017b; Nair-Menon et al., 2020). This recruitment was mediated by PLEKHA7, a ZA-specific p120-binding partner (Kourtidis et al., 2017b; Kourtidis et al., 2015; Meng et al., 2008; Pulimeno et al., 2010). We have shown that loss of junctional Ago2 localization negatively impacts Ago2-loading of a specific set of miRNAs and several of their target oncogenic mRNAs, consequently releasing RISC-mediated oncogene suppression (Kourtidis et al., 2017b; Kourtidis et al., 2015). Furthermore, we demonstrated that junctional localization of Ago2 is broadly lost in human colon tumors and in poorly differentiated colon cancer cell lines, even when cadherin junctions were still present, although not mature, implying for the existence of a mechanism fine-tuning recruitment of Ago2 to mature ZA of well-differentiated epithelia (Nair-Menon et al., 2020).

Indeed, while PLEKHA7 is required for junctional localization of Ago2, what determines Ago2's specific recruitment to the ZA is not fully known. PLEKHA7 was originally characterized

for its role in tethering the minus ends of the microtubules to the ZA (Meng et al., 2008). Notably, a significant body of work demonstrates that intracellular localization of RNA-binding complexes is mediated by the microtubule cytoskeleton (Denes et al., 2021; Kanai et al., 2004; Liao et al., 2019; Pichon et al., 2021; Scarborough et al., 2021). These observations led us to originally hypothesize that Ago2 recruitment to the ZA could be microtubule-directed. Surprisingly, our previous experimentation showed that Ago2 and PLEKHA7 localization at the ZA is microtubule-independent (Kourtidis et al., 2017b). Alternatively, the actomyosin cytoskeleton has been implicated in localization and assembly of RNA-binding complexes, such as p-bodies in the cytoplasm or Cajal bodies and the RNA-induced transcriptional gene silencing-like (RITS-like) complex in the nucleus (Ahlenstiel et al., 2012; Lindsay and McCaffrey, 2011; McCaffrey and Lindsay, 2012; Skare et al., 2003). Further, we have shown that PLEKHA7 associates with components of the actin cytoskeleton and that PLEKHA7 depletion negatively impacts integrity of the apical circumferential actin ring (Kourtidis and Anastasiadis, 2016; Kourtidis et al., 2015). This led us to ask whether recruitment of Ago2 to the ZA is actin-dependent. In this report, we show that Ago2 junctional recruitment is mediated by the actin cytoskeleton and a set of actin-interacting LIM domain-containing proteins associated with PLEKHA7 at the ZA.

Results and Discussion

PLEKHA7 and Ago2 associate with LIM domain-containing proteins at the ZA.

To obtain insight on the potential mechanisms involved in Ago2 recruitment to the ZA, we re-examined our published dataset of PLEKHA7-interacting proteins (publicly available at http://www.imexconsortium.org/; identifier: IM-25739) (Kourtidis et al., 2017b). In that experiment, PLEKHA7 immunoprecipitation from Caco2 well-differentiated intestinal epithelial cells and subsequent mass-spectrometry analysis identified more than 600 potential PLEKHA7 interactors (Kourtidis et al., 2017b). We have reported that a significant set of these interactors are RNA-binding proteins, such as RISC components (Kourtidis et al., 2017b). Here, we performed gene ontology (GO) enrichment analysis on this dataset. This analysis revealed that in addition to RNA-binding proteins, the set of PLEKHA7-associated proteins is significantly enriched for processes and functions related to the actin cytoskeleton (Fig. 1 A,B). This result aligns with our previous findings that PLEKHA7 stabilizes apical actin and that it associates with certain actin-binding proteins (Kourtidis and Anastasiadis, 2016; Kourtidis et al., 2015). Overall, the GO analyses point to RNA-binding and actin cytoskeletal-mediated functions as the top roles in which PLEKHA7 is potentially involved.

Through examining the group of actin-related PLEKHA7 interactors, we noted several proteins belonging to the LIM domain-containing protein family (Fig. 1 C). These proteins attracted our attention, since LIM protein family members, such as Ajuba, LIMD1, and WTIP, have been previously implicated in Ago2 recruitment and RISC assembly in cytoplasmic p-bodies (Bridge et al., 2017; James et al., 2010; Tilley et al., 2020). Our PLEKHA7 proteomics analysis identified a different set of proteins belonging to this same family (Fig. 1 C). More specifically, the LIM domain protein with the highest count of PLEKHA7-enriched unique peptides was LIM domain only protein 7 (LMO7) (Fig. 1 C). LMO7 was previously identified to localize to apical adherens junctions, where it plays an actin-mediated role in linking and

stabilizing nectin and cadherin junctional complexes (Ooshio et al., 2004). The other top enriched LIM domain-containing proteins were LIM and calponin homology domains-containing protein 1 (LIMCH1) and PDZ and LIM domain protein 1 (PDLIM1) (Fig. 1 C). Considering the reported functions of LIM domain-containing proteins in actin (Anderson et al., 2021; Kadrmas and Beckerle, 2004) and Ago2 regulation (Bridge et al., 2017; James et al., 2010; Tilley et al., 2020), we sought to interrogate these three LIM proteins as intermediates of Ago2 recruitment to the ZA. Protein co-immunoprecipitation, followed by Western blot analysis, confirmed PLEKHA7-LMO7-LIMCH1-PDLIM1 protein interactions with each other and with Ago2 (Fig. 1 D,E). Furthermore, immunofluorescence and confocal microscopy analysis of Caco2 monolayers revealed localization of all three LMO7, LIMCH1, and PDLIM1 distinctly to the apical ZA, similar to Ago2 localization, as determined by co-localization with mature E-cadherin adhesions and the ZA-specific marker PLEKHA7 (Kourtidis et al., 2017b; Kourtidis et al., 2015) (Fig. 1 F). Conversely, neither of these LIM proteins, Ago2, nor PLEKHA7, localize at basolateral areas of cell-cell contact (Fig. 1 G), pointing to the ZA as the subcellular location where all these proteins co-localize. Localization of LMO7 at apical AJs has been previously reported (Ooshio et al., 2004), but not that of LIMCH1 and PDLIM1, since previous studies solely focused on their roles in localizing with and modulating stress fibers, either in non-epithelial cells or in low-density conditions where cells lacked mature cell-cell junctions (Bauer et al., 2000; Lin et al., 2017; Maeda et al., 2009; Tamura et al., 2007; Vallenius et al., 2000). Together, these data point to the ZA as the subcellular compartment where PLEKHA7, Ago2, LMO7, LIMCH1, and PDLIM1 co-localize and interact; we also identify LIMCH1 and PDLIM1 as new ZA-associated LIM protein family members.

LMO7, LIMCH1, and PDLIM1 are required for recruitment of Ago2 to the ZA.

We have shown that Ago2 localization at the ZA depends on PLEKHA7 (Kourtidis et al., 2017b). Since LMO7, LIMCH1, and PDLIM1 interact with PLEKHA7 and Ago2, and all these proteins co-localize at the ZA, we asked whether any of these LIM proteins mediate Ago2 recruitment to the ZA. Strikingly, shRNA-mediated knockdown of each of these LIM proteins resulted in loss of junctional Ago2 localization, without affecting Ago2 overall levels or cytoplasmic distribution (Fig. 2 A,B). These results mirror our previous observations in PLEKHA7 knockdown cells, which we replicate here using CRISPR/Cas9-generated PLEKHA7 knockout cells, showing specific loss of junctional Ago2 localization, without changes in overall Ago2 levels or cytoplasmic distribution (Kourtidis et al., 2017b) (Fig. 2 C,D). Interestingly, knockdown of neither LMO7, LIMCH1, nor PDLIM1 had any effect on the localization or overall cellular levels of PLEKHA7 (Fig. 2 A,B), suggesting that LIM protein-mediated effects on Ago2 are downstream of PLEKHA7. In that case, PLEKHA7 knockout would be expected to also result in loss of junctional localization of these proteins, leading to loss of junctional Ago2. Intriguingly, junctional localization of neither LMO7 nor LIMCH1 are affected by PLEKHA7 knockout, but only that of PDLIM1 is lost (Fig. 2E). This result would point to PDLIM1 as the potential downstream mediator of PLEKHA7, LMO7, and LIMCH1 in recruiting Ago2 to the junctions. Still, in each of the three LIM protein knockdowns, the junctional localization of the other two LIM proteins, including that of PDLIM1, was not affected, although all knockdowns result in loss of junctional Ago2 (Fig. 2 F-H). Taken together, these results suggest that although PLEKHA7, LMO7, LIMCH1, and PDLIM1 are all required for recruitment of Ago2 to the ZA, their impact on Ago2 recruitment seems to be

independent of one another. This suggests the existence of a downstream effector linked to all these proteins that regulates Ago2 recruitment to the junctions. We sought to identify this key player next.

LMO7, LIMCH1, or PDLIM1 depletion disrupts actomyosin organization at the ZA.
LMO7, LIMCH1, and PDLIM1 have been previously reported to be involved in actomyosin organization (Bauer et al., 2000; Lin et al., 2017; Maeda et al., 2009; Ooshio et al., 2004; Tamura et al., 2007; Vallenius et al., 2000). We have also shown that PLEKHA7 knockdown disrupts the integrity of the apical circumferential actin ring (Kourtidis et al., 2015), and our GO analysis reveals actin-related functions are significantly enriched in the PLEKHA7-interacting proteome (Fig. 1 A,B). Based on these observations, we asked whether the relationship of these components with the actin cytoskeleton could be the common denominator regulating Ago2 recruitment to the ZA. First, we examined potential effects of these proteins on actomyosin organization in Caco2 cells, particularly at the ZA, where Ago2 is recruited. Using super resolution microscopy, we found that PLEKHA7 knockout cells exhibit not only a disorganized circumferential actin ring, but also loss of junctional myosin IIB (Fig. 3 A, Fig. S1 A,B), the non-muscle myosin II isoform responsible for contractile tension and actin filament stabilization at the apical actin ring (Smutny et al., 2010; Wayt et al., 2021). Super resolution microscopy also revealed that knockdown of each of LMO7, LIMCH1, and PDLIM1 had distinct, but in all cases significant effects on actomyosin organization throughout the cell and particularly at the ZA (Fig. 3 B, Fig. S1 C,D). More specifically, in LMO7 knockdown cells, apical actin filaments failed to tightly bundle into a dense cable as in control cells but remained loosely organized in dispersed actin cables (Fig. 3 B). These cells also displayed extended, widened apical myosin arrays with an appearance previously described as “sarcomeric” (Choi et al., 2016; Yu-Kemp et al., 2022). This actomyosin organization is indicative of incomplete maturation of apical actin bundles (Choi et al., 2016; Yu-Kemp et al., 2022). LIMCH1 knockdown cells showed a different pattern, where the apical filamentous actin ring is severely fragmented or completely absent (Fig. 3 B). Finally, PDLIM1 knockdown cells exhibited jagged actomyosin cables alongside bicellular junctions that appeared to be attached to intracellular actomyosin cables linked to dense cytoplasmic actomyosin aggregates (Fig. 3B - bottom panel, Fig. S1 E). This further manifested in wavy junctional cell borders and with the appearance of a distorted, collapsed apical ring structure (Fig. 3 B). Intense stress fibers were also observed in LMO7 and LIMCH1 knockdown cells (Fig. S1 D). Altogether, these results show that PLEKHA7, as well as LMO7, LIMCH1, and PDLIM1, are each distinctly responsible for the stability and homeostasis of the actomyosin cytoskeleton and particularly of the circumferential actin ring at the ZA.

Ago2 recruitment to the ZA depends on the presence of an organized actin cytoskeleton.
Since PLEKHA7, LMO7, LIMCH1, and PDLIM1 are all required for stability of the apical actomyosin cytoskeleton and for recruitment of Ago2 to the ZA, independently of each other, we asked whether proper actin organization is the underlying mechanism mediating recruitment of Ago2 to the ZA. To examine this, we utilized a classical calcium-switch assay (Gumbiner and Simons, 1986) to dismantle the calcium-dependent E-cadherin-based junctions and allow them to recover with or without the presence of Latrunculin A (LatA), an actin polymerization inhibitor (Coue et al., 1987) (Fig. 4 A). As we have previously shown (Kourtidis et

al., 2017b), E-cadherin-based junctions and the junctional localization of PLEKHA7 and Ago2, although entirely lost upon calcium depletion, fully recover within 1 hour of calcium re-introduction in control cells (Fig. 4 B-D). We also observe the same recovery time for the formation of a mature circumferential actin ring in these control cells (Fig. 4 A). These cells are entirely rounded before recovery begins, due to loss of cell-cell adhesion and actin contraction, which is marked by cytoplasmic, perinuclear actin rings (Fig. 4 A). However, as previously reported (Ivanov et al., 2004; Yu-Kemp et al., 2022), LatA-treated cells fail to round following calcium depletion, due to the lack of contraction, and pools of E-cadherin, as well as punctate actin pools, are retained at areas of cell-cell contact (Abe and Takeichi, 2008; Cavey et al., 2008; Tang and Brieher, 2012; Yamada et al., 2004) (Fig. 4 A,D). Furthermore, E-cadherin re-populates areas of cell-cell contact to re-form adherens junctions during recovery in the LatA cells, although these cells do not contain filamentous actin, again in agreement with previous observations (Ivanov et al., 2004; Tang and Brieher, 2012; Yu-Kemp et al., 2022) (Fig. 4 A). Interestingly, we also found that PLEKHA7 follows the same pattern as E-cadherin in the LatA cells, recovering at the junctions within 1 hour of calcium re-introduction (Fig. 4 C). Therefore, although PLEKHA7 is critical for the stability of the actin cytoskeleton, its localization to the junctions does not depend on the presence of organized, filamentous actin. Notably, pools of LMO7 and LIMCH1, although not of PDLIM1 that seems to be more sensitive to LatA treatment, are also retained at cell-cell junctions (Fig. 4 E-G). However, localization of Ago2 to the junctions is completely abolished in LatA-treated cells and never recovers after calcium re-addition (Fig. 4 B). These data, together with our observed effects on actin organization and Ago2 ZA recruitment by each one of PLEKHA7, LMO7, LIMCH1, and PDLIM1, demonstrate that Ago2 recruitment to the ZA depends on the presence of an organized, mature apical actin ring, downstream of all these ZA components.

Ago2 recruitment to the ZA depends on actin tension.

Our findings demonstrate that Ago2 recruitment to the ZA depends on the presence of a mature circumferential actin ring and on PLEKHA7, LMO7, LIMCH1, PDLIM1, which are all required for the stability of the actin cytoskeleton. However, we also noted that depleting each of these components had varied effects on apical actomyosin; apical actin filaments were present but dispersed in LMO7 and PDLIM1 knockdown cells (Fig. 3 B), whereas apical actin was fragmented and disorganized in LIMCH1 knockdown and PLEKHA7 knockout cells (Fig. 3 A,B). In most cases, apical actin was also notably dissociated from myosin. This is informative, since myosin monomers assemble to form an ATPase-powered motor that imposes contractile forces on the AJ-associated actin cytoskeleton (Vicente-Manzanares et al., 2009). The dissociation of apical actin and myosin in the LIM knockdown and in PLEKHA7 knockout cells, points to decreased F-actin mechanical tension (Uyeda et al., 2011). In addition, each of these cell populations display distinct cell shape changes, further suggesting disruption of tension distribution (Levayer and Lecuit, 2012) (Fig. 5 A). More specifically: a) LMO7 knockdown cells are uneven in size, with either very large or small cells observed; b) LIMCH1 knockdown cells are uniformly large and flattened; and c) PDLIM1 knockdown cells are smaller with distinct, wavy apical cell-cell borders (Fig. 5 A). Increased cell spreading and decreased contractility was previously reported in LIMCH1 knockdown cells (Lin et al., 2017). Additionally, *Drosophila* mutants lacking expression of Smallish (Smash), the fly ortholog of LMO7, also showed

junctions of unequal shape in the larval epidermis, whereas Smash overexpression resulted in increased apical constriction, suggesting a role for this LMO7 ortholog in regulating actomyosin contractility (Beati et al., 2018).

These observations led us to examine the effects of LMO7, LIMCH1, PDLIM1, and PLEKHA7 on contractile tension of the apical actin ring. To evaluate this, we used the tension-sensitive α18 antibody, which recognizes an α-catenin epitope that becomes exposed when structural changes are induced by actomyosin tension (Yonemura et al., 2010). Indeed, depletion of LMO7, LIMCH1, and PLEKHA7 disrupted actomyosin tension at the ZA, as indicated by decreased α18 intensity at bicellular junctions (Fig. 5 A,B,D,E). This reduction in α18 intensity was not observed in PDLIM1-depleted cells. However, PDLIM1-depleted cells exhibit wavy apical cell-cell borders; loss of junction straightness has also been previously associated with reduced contractile cortical tension on the junctions (Arnold et al., 2019; Sumi et al., 2018; Yamamoto et al., 2021). Indeed, measurements of bicellular junction lengths show loss of junctional straightness in PDLIM1 knockdown cells (Fig. 5 C). Notably, the distorted cell borders in PDLIM1-depleted cells resemble those observed when the cortical actomyosin-associated protein Merlin is depleted in Caco2 cells (Chiasson-MacKenzie et al., 2015). This phenotype was associated with increased contraction of the medioapical cortical cytoskeleton and reorientation of pulling forces inward, perpendicular to cell-cell junctions (Chiasson-MacKenzie et al., 2015), contrasting contraction of the circumferential actomyosin belt, which exerts pulling forces parallel to the bicellular junctions. This loss of parallel junctional tension, coupled with increased medioapical contraction, has been associated with the presence of F-actin bundles linked perpendicular to the junctions (Arnold et al., 2019), which we also noted in PDLIM1 knockdown cells (Fig. 3 B, Fig. S1 E). Altogether, these results demonstrate that PLEKHA7, LMO7, LIMCH1, and PDLIM1 are all responsible for the establishment and proper distribution of tension at the ZA.

We next asked whether contractile actomyosin tension at the ZA is indeed involved in the recruitment of Ago2 to the ZA. To examine this, we treated cells with: a) Blebbistatin, which inhibits the ATPase-dependent motor activity of myosin, but does not prevent its binding to actin (Kovacs et al., 2004); or b) the ROCK inhibitor, Y-27632, which indirectly inhibits myosin II motor activity by preventing phosphorylation of myosin II regulatory light chain (RLC) and myosin light chain phosphatase (Amano et al., 2010). We performed these treatments both in established monolayers (Fig. 5 F, Fig. S2) and during recovery, after calcium switch (Fig. 5 G-L, Fig. S3 A-F). Both Blebbistatin and Y-27632 resulted in decreased cortical actin ring tension, as indicated by disrupted actin filaments and decreased α18 signals at the ZA (Fig. 5F, Fig. S2 A,B,G,H). Concomitantly, Ago2 junctional localization was also disrupted in cells with reduced contractile tension (Fig. 5 F,G; Fig. S2 G, Fig. S3 A). The loss of Ago2 localization was more pronounced during recovery following calcium switch (Fig. 5 G, Fig. S3 A) but was also partially observed in monolayers with already established ZA (Fig. 5 F, Fig. S2 I). This is critical, showing that Ago2 localization at the ZA is sensitive to disruption of actin tension even in established mature ZA.

PLEKHA7, LMO7 and LIMCH1 localization were unaffected by Blebbistatin or ROCK inhibition (Fig. 5 I-K, Fig. S2 C-E, Fig. S3 C-E), again illustrating that the effects of actomyosin tension on Ago2 localization at the ZA are downstream of these proteins. However, PDLIM1 junctional localization was disrupted by these inhibitors (Fig. 5 L, Fig. S2 F, Fig. S5 F). This

response of PDLIM1 mirrors that observed in LatA-treated and in PLEKHA7-depleted cells, suggesting that PDLIM1 is potentially more sensitive to actin perturbations than LMO7 and LIMCH1. Interestingly, a recent study screening all members of the LIM protein family noted a specific response of PDLIM1 to tensile F-actin (Sun et al., 2020). However, PDLIM1 localization to the ZA is not affected by LMO7 or LIMCH1 knockdowns, although both result in severe effects on cortical actomyosin and in Ago2 mislocalization from the ZA. Overall, it seems that there is a complex crosstalk between LIM domain-containing proteins that warrants further investigation. However, our data demonstrate that actomyosin organization and tension at the ZA is the common critical downstream effector, directing Ago2 recruitment to the ZA.

Conclusions

Taken together, our results demonstrate that recruitment of Ago2 to the ZA is directed by the formation and maintenance of a mature, organized, tensile circumferential actin ring. This finding has three important implications. Firstly, it explains why Ago2 is specifically recruited to apical cadherin junctions at the ZA but not at basolateral cadherin contacts, as we previously demonstrated (Kourtidis et al., 2017b) and confirm in this report (Fig. 1 F,G). Secondly, it suggests that any perturbations of the circumferential actin ring, which can occur during normal processes, such as tissue morphogenesis and junctional remodeling, or aberrantly, during disease, can disrupt Ago2 localization and function. For example, it is known that aberrant actin remodeling is common in cancer, and we have shown that junctional localization of Ago2 is broadly lost in colon tumors and cancer cell lines (Hayward et al., 2021; Nair-Menon et al., 2020). These findings suggest that the mechanism instructing association of Ago2 to the ZA is broader than single protein-directed interactions. Corroborating this notion, we show here that depletion of any one of PLEKHA7, LMO7, LIMCH1, and PDLIM1 leads to disruption of both structure and tension of the apical actomyosin ring and in complete loss of Ago2 junctional localization. Thirdly, this work provides a conceptual framework, which can guide us to further study this localized RNAi function and to fully realize its significance, since we have shown that ZA-localized RNAi machinery is critical for processing and function of a set of miRNAs that regulate cell behavior (Kourtidis et al., 2017b; Kourtidis et al., 2015). In this framework, RNAi complexes at the ZA act as sensors of actomyosin contractility and organization, directly linking the mechanical state of the cell with post-transcriptional regulation of gene expression and consequently rapid modulation of cell behavior. Although more experimentation is needed to fully establish this idea, these findings introduce the concept of "mechanosensitive RNAi". In this report, we focus specifically on Ago2, however, we can also apply this approach to study the other RNA-binding proteins and complexes that we have identified at the ZA (Kourtidis et al., 2017b; Kourtidis et al., 2015) and to fully reconstruct their regulation and roles in cell and tissue homeostasis and disease.

Materials and Methods

Cell culture, generation of stable cell lines

In all comparisons, cells were used at strictly the same confluencies. All cell lines were obtained from ATCC and tested negative for mycoplasma contamination (LookOut Mycoplasma PCR Detection Kit, Sigma Aldrich). Caco2 colon epithelial cells (ATCC, #HTB-37) were cultured in

MEM (Corning) supplemented with 10% FBS (Gibco), 1 mM sodium pyruvate (Gibco), and 1X nonessential amino-acids (NEAA) solution (Gibco). HEK 293FT human embryonic kidney cells (Thermo Fisher Scientific, #R70007) were cultured in DMEM (Corning) supplemented with heat-inactivated 10% FBS, 2 mM additional L-glutamine, 1 mM sodium pyruvate, and 1X NEAA. Cells were maintained at 37°C with 5% CO_2. Lentiviral shRNA constructs were derived from the pLKO.1-based TRC1 shRNA library (Sigma-Aldrich/RNAi Consortium); the following vectors were used: pLKO.1-puro Non-Target shRNA Control, SHC016; shLMO7, TRCN0000006491; shLIMCH1, TRCN0000153799; shPDLIM1, TRCN0000161271. Lentiviral particles were produced in HEK 293FT cells co-transfected via Lipofectamine 2000 (Invitrogen) with the shRNA vector and Virapower packaging plasmids (pMDLg/pRRE, Addgene #12251; pRSV-Rev, Addgene #12253; pMD2.G, Addgene #12259) according to manufacturer instructions. shRNA lentivirus was collected and used to infect Caco2 cells according to standard protocols. Stable shRNA-expressing cell lines were maintained in 2.5 µg/ml puromycin (Gibco) following initial selection at 5 µg/ml.

The PLEKHA7 knockout Caco2 cell line was generated using CRISPR/Cas9 technology, as previously described (Ran et al., 2013). The sgRNA sequence (GGATGTTTCACTGACCATGCTGG) targeting exon 5 of PLEKHA7 was designed using the online Synthego tool (www.synthego.com) and synthesized by Integrated DNA Technologies, IDT. This PLEKHA7-targeting sgRNA was cloned into the PX459 pSPCas9(BB)-2A-Puro vector (Ran et al., 2013). Caco2 cells were transfected with 30 µg the sgRNA-containing vector using Lipofectamine 3000 (Invitrogen) according to the manufacturer's protocol. After 24 hours, cells were selected with 5 µg/ml puromycin for 48 hrs. Successfully transfected cells were seeded to obtain single colonies, which were picked and expanded for screening. PCR using primers designed to amplify the target region (Forward: CCTTTCTCAGGGCCTCATGTCA; Reverse: GCCTCCAAACAATCAGGGTTGG) was performed with DNA extracted from colonies using QuickExtract (Lucigen). PCR amplified products were screened by restriction digest analysis using the CviAII restriction enzyme (New England Biolabs). Positive candidates were sequenced to identify and confirm indels (Fig. S3 G).

Antibodies

The primary antibodies used in this study were PLEKHA7 (HPA038610; Sigma-Aldrich), E-cadherin (610182; BD Transduction Labs), Ago2 (ab57113; Abcam), Ago2 (AP5281; ECM Biosciences), LMO7 (ab224113; Abcam), LIMCH1 (ab96178; Abcam), PDLIM1 (ab129015; Abcam), β-actin (4967L; Cell Signaling Technology), Myosin IIB (909901; Biolegend). Working dilutions were 1:50 to 1:500 for immunofluorescence and 1:500 to 1:2,000 for Western blot. One exception was the polyclonal α-catenin (α18) antibody (Yonemura et al., 2010), which was a gift from Dr. Akira Nagafuchi (Nara Medical University, Japan), used at 1:4000 for immunofluorescence.

The secondary antibodies used in the present study were HRP anti–mouse (711-035-150; Jackson ImmunoResearch Laboratories), HRP anti–rabbit (711-035-152; Jackson ImmunoResearch Laboratories), Clean-Blot HRP IP Detection Reagent (21230; Thermo Fisher Scientific), Alexa Fluor 488 anti–mouse (A21202, A11029; Invitrogen), Alexa Fluor 488 anti–rabbit (A21206, A11034; Invitrogen), Alexa Fluor 488 anti–rat (A11006; Invitrogen), Alexa Fluor 594 Phalloidin (A12381; Invitrogen), Alexa Fluor 647 anti–mouse (A21236; Invitrogen), Alexa Fluor 647 anti–rabbit (A21245; Invitrogen). Working dilutions were 1:500 for

immunofluorescence and 1:2,000 for Western blot. Exceptions included: Alexa Fluor 594 Phalloidin, used at 1:100 for immunofluorescence and Clean-Blot HRP used at 1:400 when blotting for PDLIM1 in IP-eluted samples.

Immunoprecipitation

Cells were grown on 10 cm plates until fully confluent, placed on ice, washed with ice-cold PBS, and lysed with ice-cold Triton X-100 lysis buffer (150 mM NaCl, 1 mM EDTA, 50 mM Tris, pH 7.4, and 1% Triton X-100) containing 2X protease (Protease Inhibitor Cocktail III, RPI) and phosphatase inhibitors (Halt Phosphatase Inhibitor Cocktail, Thermo Scientific). Six 10 cm plates were used per IP. Prior to cell lysis, 7 µg of antibody or IgG control (011-000-003; Jackson ImmunoResearch Laboratories) was incubated with 50 µl Protein G Dynabeads (Invitrogen) in 200 µl PBS with 0.02% Tween-20 for 10-12 hrs at 4°C with constant end-to-end rotation. For the Ago2 IP, 8 µg of antibody or IgG isotype control (ab18443; Abcam) were used. After washing the antibody-conjugated beads three times with IP lysis buffer, cell lysates were incubated with the bead-conjugated antibodies 12 hrs at 4°C with constant end-to-end rotation. Beads were then washed three times with IP lysis buffer and eluted using 50 mM DTT (Sigma-Aldrich) and 0.5% SDS in lysis buffer at 58°C for 30 min, with constant agitation. Eluted proteins were separated by SDS-PAGE and analyzed by immunoblotting as described below.

Immunoblotting

Whole-cell extracts were obtained using RIPA buffer (50 mM Tris, pH 7.4, 150 mM NaCl, 1% NP-40, 0.5% deoxycholic acid, and 0.1% SDS) supplemented with protease and phosphatase inhibitors. Lysates were homogenized through a 29-G needle and cleared by full-speed centrifugation for 5 min. Protein quantification was performed using a Pierce BCA Protein Assay (Thermo Fisher Scientific). Protein extracts were mixed with Laemmli sample buffer and separated by SDS-PAGE using 4-20% TGX gels (Bio-Rad) and transferred to 0.2 µm nitrocellulose membranes (Bio-Rad) with the Trans-Blot Turbo Transfer System (Bio-Rad). Membranes were blocked and blotted in 3% milk according to standard protocols. Signals were detected by luminescence using Pierce ECL (Thermo Fisher Scientific) and a ChemiDoc Imaging System (Bio-Rad).

Immunofluorescence

Cells were grown in 12 well plates on 18 mm on sterile glass coverslips until they reached full confluence. Cells were washed once with PBS and fixed with either: a) 100% methanol (Thermo Fisher Scientific) at -20°C for 7 min; or b) 3.7% formaldehyde (Electron Microscopy Sciences) in PBS at RT for 20 min. Following 3.7% formaldehyde fixation, cells were washed 3 times with PBS + glycine (10 mM) and permeabilized for 7 min using 0.15% Triton X-100 in PBS. Cells counterstained with phalloidin to visualize F-actin were 3.7% formaldehyde fixed, while most all other cells were fixed with 100% methanol. Cells immunostained using the α18 antibody (Yonemura et al., 2010) were fixed with 1% formaldehyde in 0.1M HEPES (Gibco) at RT for 20 min, washed 3 times with PBS + glycine (10 mM), and permeabilized for 12 min using 0.15% Triton X-100 in PBS.

Cells were blocked with serum free Protein Block reagent (Dako) at RT for 1hr and stained with primary antibodies diluted in Antibody Diluent (Dako) overnight at 4°C. Cells were

then washed three times with PBS, stained with the fluorescent-labeled secondary antibodies for 1 hr at RT, washed three times with PBS, co-stained with DAPI (Sigma-Aldrich), and mounted (Aqua-Poly/Mount; Polysciences).

Imaging, image processing, and analysis

Most images were acquired using a Leica SP5 confocal microscope with a 63x Plan-Apochromat 1.4NA DIC oil immersion objective (Leica) and 405 nm, 488 nm, 594 nm, and 633 nm lasers. Image acquisition was done using Leica Application Suite Advanced Fluorescence X software at 1024 x 1024 resolution and with 0.4 µm intervals along the z-axis. For super resolution imaging, Z-series stacks were acquired in 0.4 µm intervals on a Zeiss LSM 880 NLO Quasar point scanning confocal microscope using the Airyscan detector, a 63x Plan-Apochromat 1.4NA DIC oil immersion objective (Zeiss) and the 405 nm, 488 nm, 561 nm, and 633 nm laser lines at 2024 x 2024 resolution, with 1.8X zoom. The Zeiss Zen 2.3 (black edition) software was used to control the microscope, adjust spectral detection, and for processing of the Airyscan raw images.

To allow for comparison, the same imaging parameters were used across conditions for each set of experiments. Unless otherwise noted, images are single Z-slices. In super resolution images, apical views are maximum intensity projections of the two most apical Z-slices. Quantifications were done using Fiji (Schindelin et al., 2012) (National Institutes of Health). Individual borders for measuring signal intensity or junction straightness were manually and randomly selected based on apical, crisp E-cadherin signals. Integrated α18 intensity values were measured from an 8 × 3 µm box centered on the selected cell junction in an apical Z-slice. To measure junctional straightness, the length of a line tracing the cell border from one tricellular junction to the next was compared with the length of a straight line drawn directly from one tricellular junction to another. For each of these measures 30 junctions were analyzed for each experimental condition. All statistical analyses were performed using Prism 9 (GraphPad). Unpaired two-tailed t tests were used to compare datasets consisting of two groups and one-way ANOVA was used to compare three or more groups.

Calcium switch and cytoskeletal inhibitor treatments

Caco2 cells were grown on coverslips until confluence. In Latrunculin A (LatA)-treated calcium switch assays, cells were pretreated with either DMSO (Fisher Scientific) or 10 µM LatA (Thermo Fisher Scientific) for 10 min, washed three times with calcium-free PBS, and incubated in calcium-free Caco2 medium (S-MEM; Gibco), supplemented with glutamine, 10% FBS, sodium pyruvate, NEAA, and containing 4 mM EGTA for 30 min, until cells were rounded. Calcium-free EGTA-containing medium also contained either DMSO or 10 µM LatA. Cells were then washed three times with PBS, returned to regular Caco2 medium, again with either DMSO or LatA, and fixed for immunofluorescence at the indicated time points. In Blebbistatin or Y-27632-treated calcium switch assays, there was no pre-treatment prior to incubation with calcium-free EGTA-containing Caco2 medium. Treatment was introduced in recovery, following cell rounding. In recovery, regular Caco2 medium contained either 50 µM (±)-Blebbistatin (Calbiochem)/DMSO control or 30 µM Y-27632 (Calbiochem)/water control. For static cytoskeletal inhibitor treatments, confluent cells were treated with 50 µM Blebbistatin for 3 hrs or 20 µM Y-27632 for 2 hrs.

Gene ontology enrichment analysis

The full published dataset of the 607 PLEKHA7-interacting proteins (publicly available at http://www.imexconsortium.org/; identifier: IM-25739) (Kourtidis et al., 2017b) was analyzed using the Gene Ontology (GO) Enrichment analysis online tool (http://geneontology.org) (Ashburner et al., 2000; Gene Ontology, 2021; Mi et al., 2019). Annotation version and release date of the PANTHER database used was: Reactome version 65, released 2020-11-17. Statistical analysis was performed using the PANTHER Overrepresentation Test tool. Test type used was Fisher's exact test with false discovery rate (FDR) correction. Annotation datasets used for the analysis were the PANTHER GO-slim Molecular Function and the PANTHER GO-slim Biological Process.

Supplemental material

Fig. S1 shows confocal imaging of actomyosin structures in PLEKHA7 KO and LIM protein knockdowns, as was shown in Fig. 3 by super resolution imaging; this figure also provides supplemental basal z-slices and a maximum intensity projection through the entire acquired Z-plane for the shPDLIM1 super resolution field shown in Fig. 3 B. Fig. S2 shows α18, PLEKHA7, and LIM protein immunofluorescence in Blebbistatin-treated confluent Caco2 monolayers, as well as α18 and Ago2 immunofluorescence in Y-27632-treated confluent Caco2 monolayers. Fig. S3 shows immunofluorescence of junctional markers, Ago2, and LIM proteins during a calcium switch assay with or without Y-27632 treatment during recovery; it also includes sequencing confirmation of CRISPR/Cas9 - mediated genomic deletions to generate PLEKHA7 knockout Caco2 cells.

Acknowledgements

We would like to thank Dr. Akira Nagafuchi, Nara Medical University, Japan, for kindly providing the α18 antibody; Drs. Christiana Kappler and Stephen Duncan, Cell Models Core, Digestive Disease Research Core Center, MUSC (NIH P30 DK123704) for support with CRISPR/Cas9 reagents; Drs. Li Li and John Lemasters, Advanced Imaging Core, Digestive Disease Research Core Center, MUSC (NIH P30 DK123704) for support with super resolution microscopy; Dr. David Turner and the shRNA Technology Shared Resource, Hollings Cancer Center, MUSC (NIH P30 CA138313) for providing shRNA constructs.

This work was supported by NIH grants R01 DK124553, R21 CA246233, P20 GM130457, P20 GM103499-21S1, and P30 DK123704 to AK. MCB was supported by NIH training grants TL1 TR001451 and UL1 TR001450.

The authors declare no competing financial interests.

Author contributions: Conceptualization: MCB, AK; data acquisition: MCB, JNM, MED; data analysis: MCB, AK; writing - original draft: MCB; writing - review and editing: MCB, AK

References

Abe, K., and M. Takeichi. 2008. EPLIN mediates linkage of the cadherin catenin complex to F-actin and stabilizes the circumferential actin belt. *Proceedings of the National Academy of Sciences of the United States of America*. 105:13-19.

Ahlenstiel, C.L., H.G. Lim, D.A. Cooper, T. Ishida, A.D. Kelleher, and K. Suzuki. 2012. Direct evidence of nuclear Argonaute distribution during transcriptional silencing links the actin cytoskeleton to nuclear RNAi machinery in human cells. *Nucleic acids research*. 40:1579-1595.

Amano, M., M. Nakayama, and K. Kaibuchi. 2010. Rho-kinase/ROCK: A key regulator of the cytoskeleton and cell polarity. *Cytoskeleton (Hoboken)*. 67:545-554.

Anderson, C.A., D.R. Kovar, M.L. Gardel, and J.D. Winkelman. 2021. LIM domain proteins in cell mechanobiology. *Cytoskeleton (Hoboken)*. 78:303-311.

Antoniou, A., M. Baptista, N. Carney, and J.G. Hanley. 2014. PICK1 links Argonaute 2 to endosomes in neuronal dendrites and regulates miRNA activity. *EMBO reports*. 15:548-556.

Arnold, T.R., J.H. Shawky, R.E. Stephenson, K.M. Dinshaw, T. Higashi, F. Huq, L.A. Davidson, and A.L. Miller. 2019. Anillin regulates epithelial cell mechanics by structuring the medial-apical actomyosin network. *Elife*. 8.

Ashburner, M., C.A. Ball, J.A. Blake, D. Botstein, H. Butler, J.M. Cherry, A.P. Davis, K. Dolinski, S.S. Dwight, J.T. Eppig, M.A. Harris, D.P. Hill, L. Issel-Tarver, A. Kasarskis, S. Lewis, J.C. Matese, J.E. Richardson, M. Ringwald, G.M. Rubin, and G. Sherlock. 2000. Gene ontology: tool for the unification of biology. The Gene Ontology Consortium. *Nat Genet*. 25:25-29.

Bauer, K., M. Kratzer, M. Otte, K.L. de Quintana, J. Hagmann, G.J. Arnold, C. Eckerskorn, F. Lottspeich, and W. Siess. 2000. Human CLP36, a PDZ-domain and LIM-domain protein, binds to alpha-actinin-1 and associates with actin filaments and stress fibers in activated platelets and endothelial cells. *Blood*. 96:4236-4245.

Beati, H., I. Peek, P. Hordowska, M. Honemann-Capito, J. Glashauser, F.A. Renschler, P. Kakanj, A. Ramrath, M. Leptin, S. Luschnig, S. Wiesner, and A. Wodarz. 2018. The adherens junction-associated LIM domain protein Smallish regulates epithelial morphogenesis. *The Journal of cell biology*. 217:1079-1095.

Bose, M., S. Chatterjee, Y. Chakrabarty, B. Barman, and S.N. Bhattacharyya. 2020. Retrograde trafficking of Argonaute 2 acts as a rate-limiting step for de novo miRNP formation on endoplasmic reticulum-attached polysomes in mammalian cells. *Life Sci Alliance*. 3.

Bridge, K.S., K.M. Shah, Y. Li, D.E. Foxler, S.C.K. Wong, D.C. Miller, K.M. Davidson, J.G. Foster, R. Rose, M.R. Hodgkinson, P.S. Ribeiro, A.A. Aboobaker, K. Yashiro, X. Wang, P.R. Graves, M.J. Plevin, D. Lagos, and T.V. Sharp. 2017. Argonaute Utilization for miRNA Silencing Is Determined by Phosphorylation-Dependent Recruitment of LIM-Domain-Containing Proteins. *Cell Rep*. 20:173-187.

Cavey, M., M. Rauzi, P.F. Lenne, and T. Lecuit. 2008. A two-tiered mechanism for stabilization and immobilization of E-cadherin. *Nature*. 453:751-756.

Chiasson-MacKenzie, C., Z.S. Morris, Q. Baca, B. Morris, J.K. Coker, R. Mirchev, A.E. Jensen, T. Carey, S.L. Stott, D.E. Golan, and A.I. McClatchey. 2015. NF2/Merlin mediates contact-

dependent inhibition of EGFR mobility and internalization via cortical actomyosin. *The Journal of cell biology*. 211:391-405.

Choi, W., B.R. Acharya, G. Peyret, M.A. Fardin, R.M. Mege, B. Ladoux, A.S. Yap, A.S. Fanning, and M. Peifer. 2016. Remodeling the zonula adherens in response to tension and the role of afadin in this response. *The Journal of cell biology*. 213:243-260.

Coue, M., S.L. Brenner, I. Spector, and E.D. Korn. 1987. Inhibition of actin polymerization by latrunculin A. *FEBS letters*. 213:316-318.

Daulagala, A.C., M.C. Bridges, and A. Kourtidis. 2019. E-cadherin Beyond Structure: A Signaling Hub in Colon Homeostasis and Disease. *Int J Mol Sci*. 20.

Denes, L.T., C.P. Kelley, and E.T. Wang. 2021. Microtubule-based transport is essential to distribute RNA and nascent protein in skeletal muscle. *Nat Commun*. 12:6079.

Detzer, A., C. Engel, W. Wunsche, and G. Sczakiel. 2011. Cell stress is related to re-localization of Argonaute 2 and to decreased RNA interference in human cells. *Nucleic acids research*. 39:2727-2741.

Farquhar, M.G., and G.E. Palade. 1963. Junctional complexes in various epithelia. *The Journal of cell biology*. 17:375-412.

Gagnon, K.T., L. Li, Y. Chu, B.A. Janowski, and D.R. Corey. 2014. RNAi factors are present and active in human cell nuclei. *Cell Rep*. 6:211-221.

Gene Ontology, C. 2021. The Gene Ontology resource: enriching a GOld mine. *Nucleic acids research*. 49:D325-D334.

Gumbiner, B., and K. Simons. 1986. A functional assay for proteins involved in establishing an epithelial occluding barrier: identification of a uvomorulin-like polypeptide. *The Journal of cell biology*. 102:457-468.

Hammond, S.M., S. Boettcher, A.A. Caudy, R. Kobayashi, and G.J. Hannon. 2001. Argonaute2, a link between genetic and biochemical analyses of RNAi. *Science (New York, N.Y*. 293:1146-1150.

Harris, T.J., and U. Tepass. 2010. Adherens junctions: from molecules to morphogenesis. *Nat Rev Mol Cell Biol*. 11:502-514.

Hayward, M.K., J.M. Muncie, and V.M. Weaver. 2021. Tissue mechanics in stem cell fate, development, and cancer. *Developmental cell*. 56:1833-1847.

Huntzinger, E., and E. Izaurralde. 2011. Gene silencing by microRNAs: contributions of translational repression and mRNA decay. *Nat Rev Genet*. 12:99-110.

Ivanov, A.I., I.C. McCall, C.A. Parkos, and A. Nusrat. 2004. Role for actin filament turnover and a myosin II motor in cytoskeleton-driven disassembly of the epithelial apical junctional complex. *Molecular biology of the cell*. 15:2639-2651.

James, V., Y. Zhang, D.E. Foxler, C.H. de Moor, Y.W. Kong, T.M. Webb, T.J. Self, Y. Feng, D. Lagos, C.Y. Chu, T.M. Rana, S.J. Morley, G.D. Longmore, M. Bushell, and T.V. Sharp. 2010. LIM-domain proteins, LIMD1, Ajuba, and WTIP are required for microRNA-mediated gene silencing. *Proceedings of the National Academy of Sciences of the United States of America*. 107:12499-12504.

Kadrmas, J.L., and M.C. Beckerle. 2004. The LIM domain: from the cytoskeleton to the nucleus. *Nat Rev Mol Cell Biol*. 5:920-931.

Kanai, Y., N. Dohmae, and N. Hirokawa. 2004. Kinesin transports RNA: isolation and characterization of an RNA-transporting granule. *Neuron*. 43:513-525.

Kourtidis, A., and P.Z. Anastasiadis. 2016. PLEKHA7 defines an apical junctional complex with cytoskeletal associations and miRNA-mediated growth implications. *Cell cycle (Georgetown, Tex*. 15:498-505.

Kourtidis, A., R. Lu, L.J. Pence, and P.Z. Anastasiadis. 2017a. A central role for cadherin signaling in cancer. *Experimental cell research*. 358:78-85.

Kourtidis, A., B. Necela, W.H. Lin, R. Lu, R.W. Feathers, Y.W. Asmann, E.A. Thompson, and P.Z. Anastasiadis. 2017b. Cadherin complexes recruit mRNAs and RISC to regulate epithelial cell signaling. *The Journal of cell biology*. 216:3073-3085.

Kourtidis, A., S.P. Ngok, and P.Z. Anastasiadis. 2013. p120 catenin: an essential regulator of cadherin stability, adhesion-induced signaling, and cancer progression. *Prog Mol Biol Transl Sci*. 116:409-432.

Kourtidis, A., S.P. Ngok, P. Pulimeno, R.W. Feathers, L.R. Carpio, T.R. Baker, J.M. Carr, I.K. Yan, S. Borges, E.A. Perez, P. Storz, J.A. Copland, T. Patel, E.A. Thompson, S. Citi, and P.Z. Anastasiadis. 2015. Distinct E-cadherin-based complexes regulate cell behaviour through miRNA processing or Src and p120 catenin activity. *Nature cell biology*. 17:1145-1157.

Kovacs, E.M., M. Goodwin, R.G. Ali, A.D. Paterson, and A.S. Yap. 2002. Cadherin-directed actin assembly: E-cadherin physically associates with the Arp2/3 complex to direct actin assembly in nascent adhesive contacts. *Curr Biol*. 12:379-382.

Kovacs, E.M., S. Verma, R.G. Ali, A. Ratheesh, N.A. Hamilton, A. Akhmanova, and A.S. Yap. 2011. N-WASP regulates the epithelial junctional actin cytoskeleton through a non-canonical post-nucleation pathway. *Nature cell biology*. 13:934-943.

Kovacs, M., J. Toth, C. Hetenyi, A. Malnasi-Csizmadia, and J.R. Sellers. 2004. Mechanism of blebbistatin inhibition of myosin II. *The Journal of biological chemistry*. 279:35557-35563.

Leerberg, J.M., G.A. Gomez, S. Verma, E.J. Moussa, S.K. Wu, R. Priya, B.D. Hoffman, C. Grashoff, M.A. Schwartz, and A.S. Yap. 2014. Tension-sensitive actin assembly supports contractility at the epithelial zonula adherens. *Curr Biol*. 24:1689-1699.

Leung, A.K., J.M. Calabrese, and P.A. Sharp. 2006. Quantitative analysis of Argonaute protein reveals microRNA-dependent localization to stress granules. *Proc. Natl. Acad. Sci. USA*. 103:18125-18130.

Levayer, R., and T. Lecuit. 2012. Biomechanical regulation of contractility: spatial control and dynamics. *Trends in cell biology*. 22:61-81.

Liao, Y.C., M.S. Fernandopulle, G. Wang, H. Choi, L. Hao, C.M. Drerup, R. Patel, S. Qamar, J. Nixon-Abell, Y. Shen, W. Meadows, M. Vendruscolo, T.P.J. Knowles, M. Nelson, M.A. Czekalska, G. Musteikyte, M.A. Gachechiladze, C.A. Stephens, H.A. Pasolli, L.R. Forrest, P. St George-Hyslop, J. Lippincott-Schwartz, and M.E. Ward. 2019. RNA Granules Hitchhike on Lysosomes for Long-Distance Transport, Using Annexin A11 as a Molecular Tether. *Cell*. 179:147-164 e120.

Lin, Y.H., Y.Y. Zhen, K.Y. Chien, I.C. Lee, W.C. Lin, M.Y. Chen, and L.M. Pai. 2017. LIMCH1 regulates nonmuscle myosin-II activity and suppresses cell migration. *Molecular biology of the cell*. 28:1054-1065.

Lindsay, A.J., and M.W. McCaffrey. 2011. Myosin Va is required for P body but not stress granule formation. *The Journal of biological chemistry*. 286:11519-11528.

Liu, J., M.A. Carmell, F.V. Rivas, C.G. Marsden, J.M. Thomson, J.J. Song, S.M. Hammond, L. Joshua-Tor, and G.J. Hannon. 2004. Argonaute2 is the catalytic engine of mammalian RNAi. *Science (New York, N.Y*. 305:1437-1441.

Maeda, M., E. Asano, D. Ito, S. Ito, Y. Hasegawa, M. Hamaguchi, and T. Senga. 2009. Characterization of interaction between CLP36 and palladin. *The FEBS journal*. 276:2775-2785.

McCaffrey, M.W., and A.J. Lindsay. 2012. Roles for myosin Va in RNA transport and turnover. *Biochem Soc Trans*. 40:1416-1420.

Mege, R.M., and N. Ishiyama. 2017. Integration of Cadherin Adhesion and Cytoskeleton at Adherens Junctions. *Cold Spring Harb Perspect Biol*. 9.

Meister, G., M. Landthaler, A. Patkaniowska, Y. Dorsett, G. Teng, and T. Tuschl. 2004. Human Argonaute2 mediates RNA cleavage targeted by miRNAs and siRNAs. *Molecular cell*. 15:185-197.

Mendonsa, A.M., T.Y. Na, and B.M. Gumbiner. 2018. E-cadherin in contact inhibition and cancer. *Oncogene*. 37:4769-4780.

Meng, W., Y. Mushika, T. Ichii, and M. Takeichi. 2008. Anchorage of microtubule minus ends to adherens junctions regulates epithelial cell-cell contacts. *Cell*. 135:948-959.

Meng, W., and M. Takeichi. 2009. Adherens junction: molecular architecture and regulation. *Cold Spring Harb Perspect Biol*. 1:a002899.

Mi, H., A. Muruganujan, D. Ebert, X. Huang, and P.D. Thomas. 2019. PANTHER version 14: more genomes, a new PANTHER GO-slim and improvements in enrichment analysis tools. *Nucleic acids research*. 47:D419-D426.

Nair-Menon, J., A.C. Daulagala, D.M. Connor, L. Rutledge, T. Penix, M.C. Bridges, B. Wellslager, D.D. Spyropoulos, C.D. Timmers, A.M. Broome, and A. Kourtidis. 2020. Predominant Distribution of the RNAi Machinery at Apical Adherens Junctions in Colonic Epithelia Is Disrupted in Cancer. *Int J Mol Sci*. 21.

Ooshio, T., K. Irie, K. Morimoto, A. Fukuhara, T. Imai, and Y. Takai. 2004. Involvement of LMO7 in the association of two cell-cell adhesion molecules, nectin and E-cadherin, through afadin and alpha-actinin in epithelial cells. *The Journal of biological chemistry*. 279:31365-31373.

Pichon, X., K. Moissoglu, E. Coleno, T. Wang, A. Imbert, M.C. Robert, M. Peter, R. Chouaib, T. Walter, F. Mueller, K. Zibara, E. Bertrand, and S. Mili. 2021. The kinesin KIF1C transports APC-dependent mRNAs to cell protrusions. *RNA (New York, N.Y*. 27:1528-1544.

Priya, R., A.S. Yap, and G.A. Gomez. 2013. E-cadherin supports steady-state Rho signaling at the epithelial zonula adherens. *Differentiation; research in biological diversity*. 86:133-140.

Pulimeno, P., C. Bauer, J. Stutz, and S. Citi. 2010. PLEKHA7 is an adherens junction protein with a tissue distribution and subcellular localization distinct from ZO-1 and E-cadherin. *PloS one*. 5:e12207.

Ramirez Moreno, M., and N.A. Bulgakova. 2021. The Cross-Talk Between EGFR and E-Cadherin. *Frontiers in cell and developmental biology*. 9:828673.

Ran, F.A., P.D. Hsu, J. Wright, V. Agarwala, D.A. Scott, and F. Zhang. 2013. Genome engineering using the CRISPR-Cas9 system. *Nature protocols*. 8:2281-2308.

Ratheesh, A., and A.S. Yap. 2012. A bigger picture: classical cadherins and the dynamic actin cytoskeleton. *Nature reviews. Molecular cell biology*. 13:673-679.

Reynolds, A.B., J. Daniel, P.D. McCrea, M.J. Wheelock, J. Wu, and Z. Zhang. 1994. Identification of a new catenin: the tyrosine kinase substrate p120cas associates with E-cadherin complexes. *Molecular and cellular biology*. 14:8333-8342.

Salvi, A.M., and K.A. DeMali. 2018. Mechanisms linking mechanotransduction and cell metabolism. *Current opinion in cell biology*. 54:114-120.

Scarborough, E.A., K. Uchida, M. Vogel, N. Erlitzki, M. Iyer, S.A. Phyo, A. Bogush, I. Kehat, and B.L. Prosser. 2021. Microtubules orchestrate local translation to enable cardiac growth. *Nat Commun*. 12:1547.

Schindelin, J., I. Arganda-Carreras, E. Frise, V. Kaynig, M. Longair, T. Pietzsch, S. Preibisch, C. Rueden, S. Saalfeld, B. Schmid, J.Y. Tinevez, D.J. White, V. Hartenstein, K. Eliceiri, P. Tomancak, and A. Cardona. 2012. Fiji: an open-source platform for biological-image analysis. *Nat Methods*. 9:676-682.

Shewan, A.M., M. Maddugoda, A. Kraemer, S.J. Stehbens, S. Verma, E.M. Kovacs, and A.S. Yap. 2005. Myosin 2 is a key Rho kinase target necessary for the local concentration of E-cadherin at cell-cell contacts. *Molecular biology of the cell*. 16:4531-4542.

Skare, P., J.P. Kreivi, A. Bergstrom, and R. Karlsson. 2003. Profilin I colocalizes with speckles and Cajal bodies: a possible role in pre-mRNA splicing. *Experimental cell research*. 286:12-21.

Smutny, M., H.L. Cox, J.M. Leerberg, E.M. Kovacs, M.A. Conti, C. Ferguson, N.A. Hamilton, R.G. Parton, R.S. Adelstein, and A.S. Yap. 2010. Myosin II isoforms identify distinct functional modules that support integrity of the epithelial zonula adherens. *Nature cell biology*. 12:696-702.

Sumi, A., P. Hayes, A. D'Angelo, J. Colombelli, G. Salbreux, K. Dierkes, and J. Solon. 2018. Adherens Junction Length during Tissue Contraction Is Controlled by the Mechanosensitive Activity of Actomyosin and Junctional Recycling. *Developmental cell*. 47:453-463 e453.

Sun, X., D.Y.Z. Phua, L. Axiotakis, Jr., M.A. Smith, E. Blankman, R. Gong, R.C. Cail, S. Espinosa de Los Reyes, M.C. Beckerle, C.M. Waterman, and G.M. Alushin. 2020. Mechanosensing through Direct Binding of Tensed F-Actin by LIM Domains. *Developmental cell*. 55:468-482 e467.

Takeichi, M. 1995. Morphogenetic roles of classic cadherins. *Curr. Opin. in Cell Biol.* 7:619-627.

Takeichi, M. 2014. Dynamic contacts: rearranging adherens junctions to drive epithelial remodelling. *Nat Rev Mol Cell Biol*. 15:397-410.

Tamura, N., K. Ohno, T. Katayama, N. Kanayama, and K. Sato. 2007. The PDZ-LIM protein CLP36 is required for actin stress fiber formation and focal adhesion assembly in BeWo cells. *Biochemical and biophysical research communications*. 364:589-594.

Tang, V.W., and W.M. Brieher. 2012. alpha-Actinin-4/FSGS1 is required for Arp2/3-dependent actin assembly at the adherens junction. *The Journal of cell biology*. 196:115-130.

Thoreson, M.A., P.Z. Anastasiadis, J.M. Daniel, R.C. Ireton, M.J. Wheelock, K.R. Johnson, D.K. Hummingbird, and A.B. Reynolds. 2000. Selective uncoupling of p120(ctn) from E-cadherin disrupts strong adhesion. *The Journal of cell biology*. 148:189-202.

Tilley, A.M.C., C.M. Howard, S. Sridharan, B. Subramaniyan, N.R. Bearss, S. Alkhalili, and D. Raman. 2020. The CXCR4-Dependent LASP1-Ago2 Interaction in Triple-Negative Breast Cancer. *Cancers (Basel)*. 12.

Uyeda, T.Q., Y. Iwadate, N. Umeki, A. Nagasaki, and S. Yumura. 2011. Stretching actin filaments within cells enhances their affinity for the myosin II motor domain. *PloS one*. 6:e26200.

Vallenius, T., K. Luukko, and T.P. Makela. 2000. CLP-36 PDZ-LIM protein associates with nonmuscle alpha-actinin-1 and alpha-actinin-4. *The Journal of biological chemistry*. 275:11100-11105.

Verma, S., S.P. Han, M. Michael, G.A. Gomez, Z. Yang, R.D. Teasdale, A. Ratheesh, E.M. Kovacs, R.G. Ali, and A.S. Yap. 2012. A WAVE2-Arp2/3 actin nucleator apparatus supports junctional tension at the epithelial zonula adherens. *Molecular biology of the cell*. 23:4601-4610.

Vicente-Manzanares, M., X. Ma, R.S. Adelstein, and A.R. Horwitz. 2009. Non-muscle myosin II takes centre stage in cell adhesion and migration. *Nat Rev Mol Cell Biol*. 10:778-790.

Wayt, J., A. Cartagena-Rivera, D. Dutta, J.G. Donaldson, and C.M. Waterman. 2021. Myosin II isoforms promote internalization of spatially distinct clathrin-independent endocytosis cargoes through modulation of cortical tension downstream of ROCK2. *Molecular biology of the cell*. 32:226-236.

Yamada, A., K. Irie, A. Fukuhara, T. Ooshio, and Y. Takai. 2004. Requirement of the actin cytoskeleton for the association of nectins with other cell adhesion molecules at adherens and tight junctions in MDCK cells. *Genes Cells*. 9:843-855.

Yamada, S., and W.J. Nelson. 2007. Localized zones of Rho and Rac activities drive initiation and expansion of epithelial cell-cell adhesion. *The Journal of cell biology*. 178:517-527.

Yamamoto, K., H. Miura, M. Ishida, Y. Mii, N. Kinoshita, S. Takada, N. Ueno, S. Sawai, Y. Kondo, and K. Aoki. 2021. Optogenetic relaxation of actomyosin contractility uncovers mechanistic roles of cortical tension during cytokinesis. *Nat Commun*. 12:7145.

Yonemura, S., Y. Wada, T. Watanabe, A. Nagafuchi, and M. Shibata. 2010. alpha-Catenin as a tension transducer that induces adherens junction development. *Nature cell biology*. 12:533-542.

Yu-Kemp, H.C., R.A. Szymanski, D.B. Cortes, N.C. Gadda, M.L. Lillich, A.S. Maddox, and M. Peifer. 2022. Micron-scale supramolecular myosin arrays help mediate cytoskeletal assembly at mature adherens junctions. *The Journal of cell biology*. 221.

Yu, Y., and R.C. Elble. 2016. Homeostatic Signaling by Cell-Cell Junctions and Its Dysregulation during Cancer Progression. *J Clin Med*. 5.

Yulis, M., D.H.M. Kusters, and A. Nusrat. 2018. Cadherins: cellular adhesive molecules serving as signalling mediators. *J Physiol*. 596:3883-3898.

Zeng, Y., H. Sankala, X. Zhang, and P.R. Graves. 2008. Phosphorylation of Argonaute 2 at serine-387 facilitates its localization to processing bodies. *The Biochemical journal*. 413:429-436.

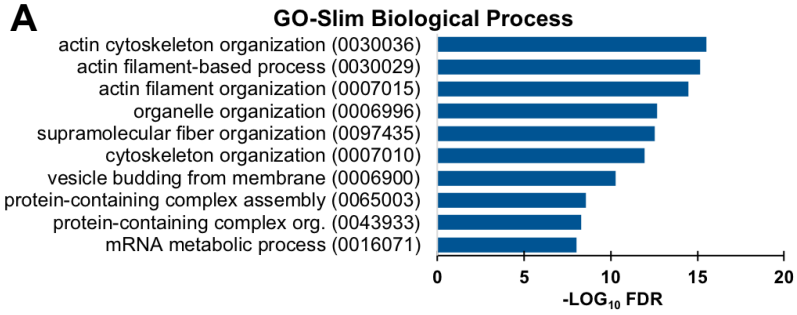

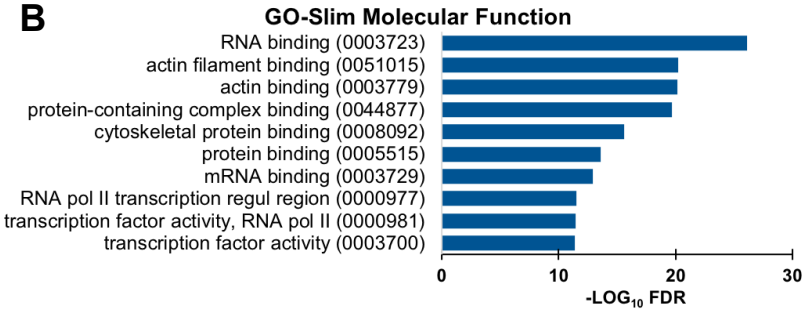

C

Gene ID	Gene name	Unique peptides
LMO7	LIM domain only protein 7	53
LIMCH1	LIM and calponin homology domains-containing protein 1	17
PDLIM1	PDZ and LIM domain protein 1	14
LIMA	LIM domain and actin-binding protein 1	6
LASP	LIM and SH3 domain protein 1	5

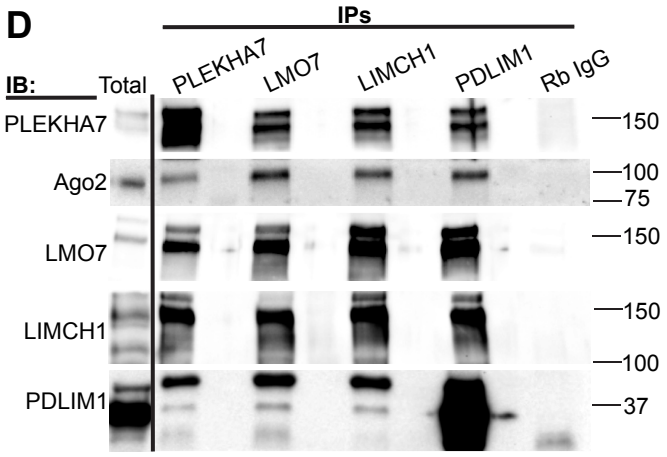

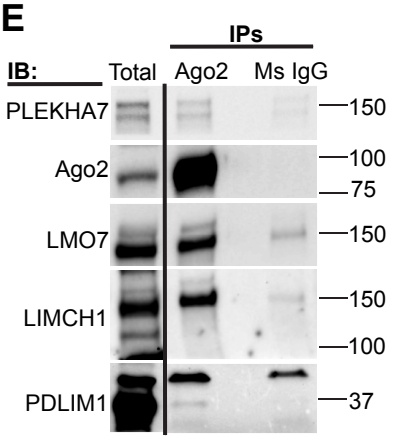

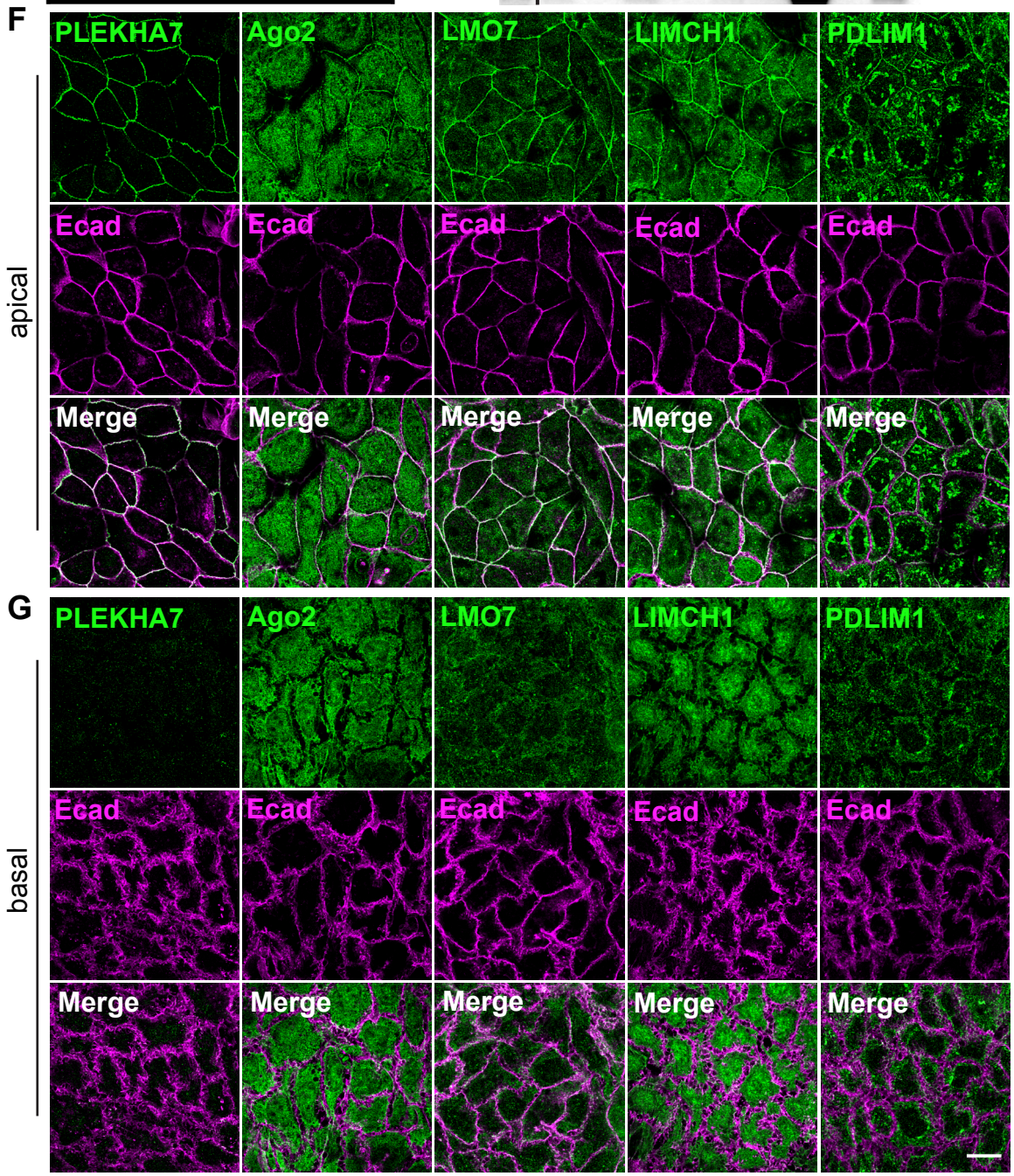

Fig. 1

Figure 1. PLEKHA7 interacts with Ago2 and actin-related, LIM domain-containing proteins at apical adherens junctions. (A, B) Gene ontology (GO) enrichment analyses of the PLEKHA7-interacting protein dataset (http://www.imexconsortium.org/; identifier: IM-25739). The GO-slim Molecular Function and GO-slim Biological Process datasets were interrogated using Fisher's exact test with false discovery rate (FDR) correction to assess enrichment significance. The 10 most significantly enriched GO terms are shown; GO term accession numbers are displayed in parentheses. **(C)** LIM domain-containing proteins identified in the same dataset of PLEKHA7 interactors; the unique peptide counts recorded from mass spectrometry analysis following PLEKHA7 immunoprecipitation are shown. **(D, E)** Immunoprecipitation (IP) of PLEKHA7, LMO7, LIMCH1, PDLIM1 and Ago2 from Caco2 cells, immunoblotted (IB) for the same markers; IgG is the negative control. Molecular masses (kD) are indicated on the right. **(F, G)** Immunofluorescence of E-cadherin (Ecad), PLEKHA7, LMO7, LIMCH1, PDLIM1 and Ago2 in confluent Caco2 cell monolayers. Images were obtained by confocal microscopy, and Z-series stacks were acquired through the entire plane; representative apical **(F)** and basal **(G)** Z-slices are shown. Scale bar = 20 µm.

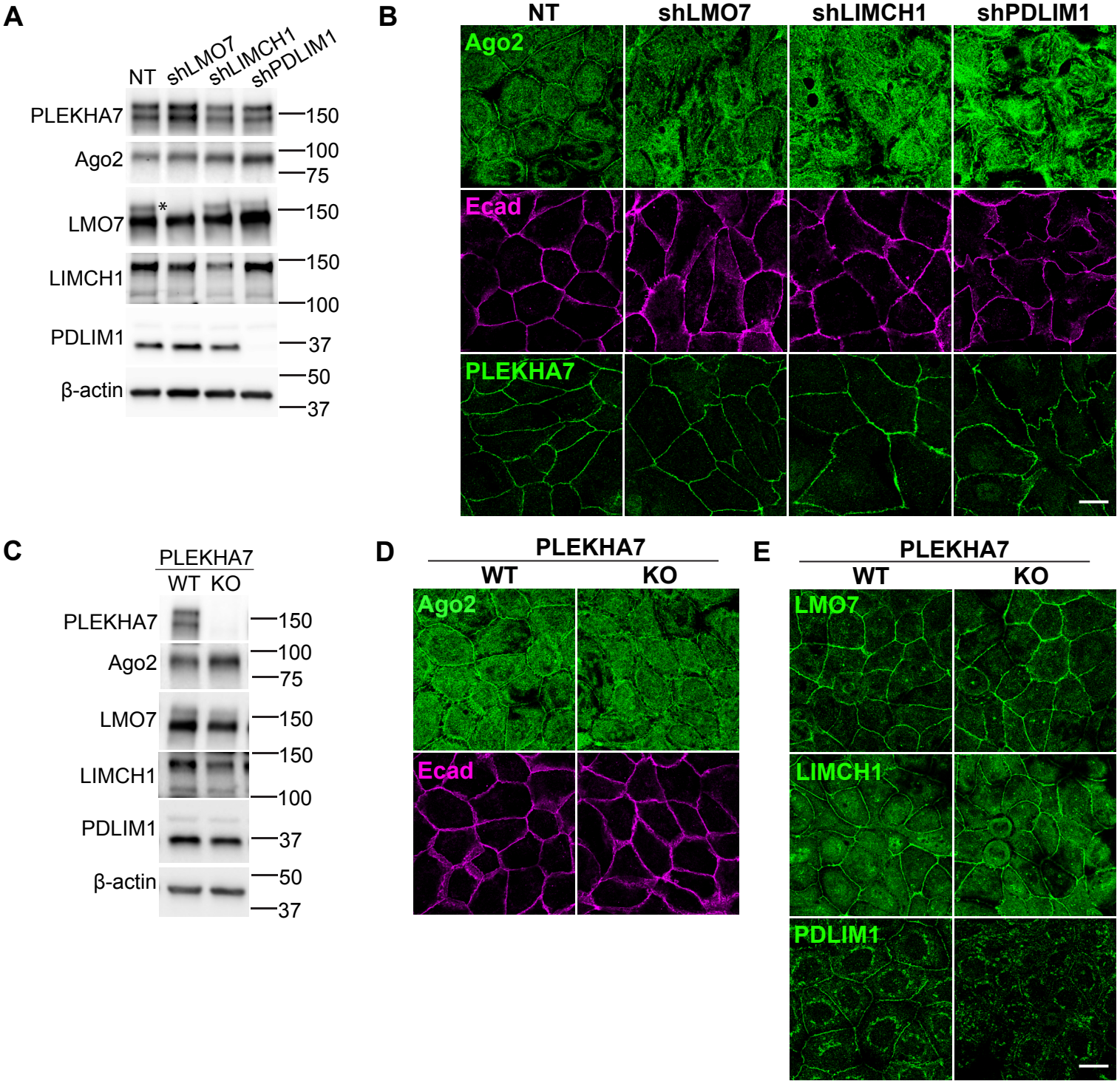
A
NT
shLMO7
shLIMCH1
shPDLIM1
PLEKHA7
Ago2
LMO7
LIMCH1
PDLIM1
β-actin
150
100
75
150
150
100
37
50
37
*
B
NT
shLMO7
shLIMCH1
shPDLIM1
Ago2
Ecad
PLEKHA7
C
PLEKHA7
WT
KO
PLEKHA7
Ago2
LMO7
LIMCH1
PDLIM1
β-actin
150
100
75
150
150
100
37
50
37
D
PLEKHA7
WT
KO
Ago2
Ecad
E
PLEKHA7
WT
KO
LMO7
LIMCH1
PDLIM1
F
NT
shLMO7
LIMCH1
PDLIM1
G
NT
shLIMCH1
LMO7
PDLIM1
H
NT
shPDLIM1
LMO7
LIMCH1

Fig. 2

Figure 2. LMO7, LIMCH1, PDLIM1, and PLEKHA7 loss each specifically disrupt junctional localization of Ago2. (A) Immunoblotting of LMO7, LIMCH1, and PDLIM1 shRNA-mediated knockdown (shLMO7, shLIMCH1, shPDLIM1, respectively) Caco2 cells, compared to non-target (NT) shRNA control cells; asterisk indicates the specific LMO7 band lost by shRNA targeting. **(B)** Immunofluorescence of shLMO7, shLIMCH1, shPDLIM1 Caco2 cells for Ago2, PLEKHA7, and E-cadherin (Ecad). **(C)** Immunoblotting of PLEKHA7 knockout (KO) Caco2 cells, compared to control wild type cells (WT). **(D, E)** Immunofluorescence of control (WT) or PLEKHA7 knockout (KO) cells for Ago2, LMO7, LIMCH1, PDLIM1, and E-cadherin (Ecad). **(F-H)** Immunofluorescence of each LMO7, LIMCH1, and PDLIM1 in shLMO7, shLIMCH1, shPDLIM1 Caco2 cells. In all immunoblots, β-actin is the loading control; molecular masses (kD) are indicated on the right. For all figures, unless indicated, top-view immunofluorescence images were obtained by confocal microscopy and are single apical Z-slices. Scale bars = 20 µm.

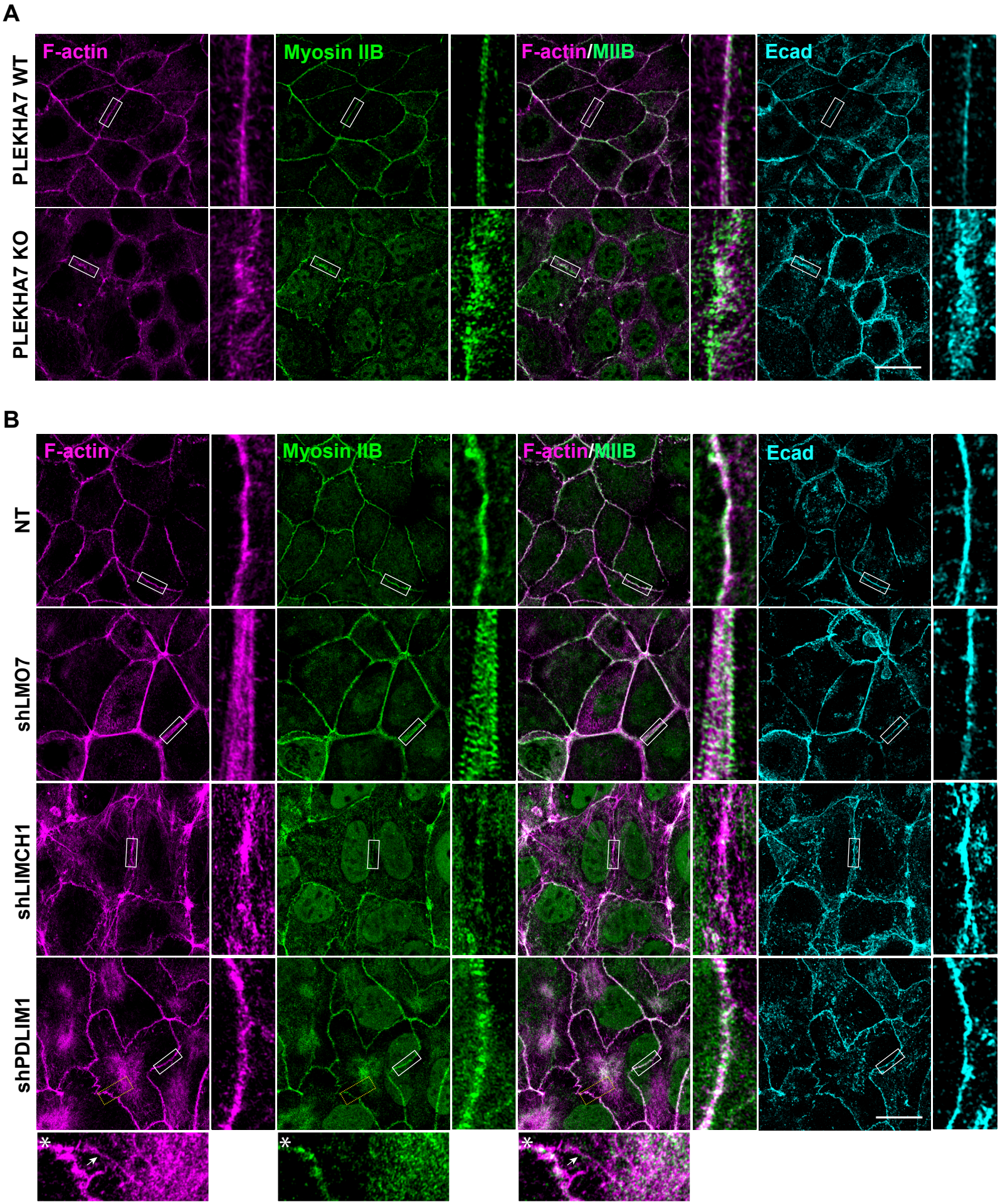
A
F-actin
Myosin IIB
F-actin/MIIB
Ecad
PLEKHA7 WT
PLEKHA7 KO
B
F-actin
Myosin IIB
F-actin/MIIB
Ecad
NT
shLMO7
shLIMCH1
shPDLIM1

Fig. 3

Figure 3. PLEKHA7, LMO7, LIMCH1, and PDLIM1 each distinctly influence apical actomyosin organization. (A) Immunofluorescence (IF) and super resolution microscopy of PLEKHA7 knockout (KO) Caco2 cells compared to control wild type (WT) Caco2 cells **(B)** IF and super resolution microscopy of LMO7, LIMCH1, and PDLIM1 knockdown (shLMO7, shLIMCH1, shPDLIM1) Caco2 cells, compared to (NT) shRNA control cells. Top-view immunofluorescence images are maximum intensity projections of the two most apical Z-slices. Insets marked by white rectangles are 6X magnification of the original image. Insets for shPDLIM1 cells noted with asterisks are magnified 5X from areas marked with yellow dashed boxes. Asterisk marked insets are from full maximum intensity projection images (see Fig. S2) to indicate basolateral actin filaments linked to the apical actin ring (marked by white arrows). Scale bars = 20 µm. In all cases, E-cadherin (Ecad) is used as a co-stain denoting adherens junctions.

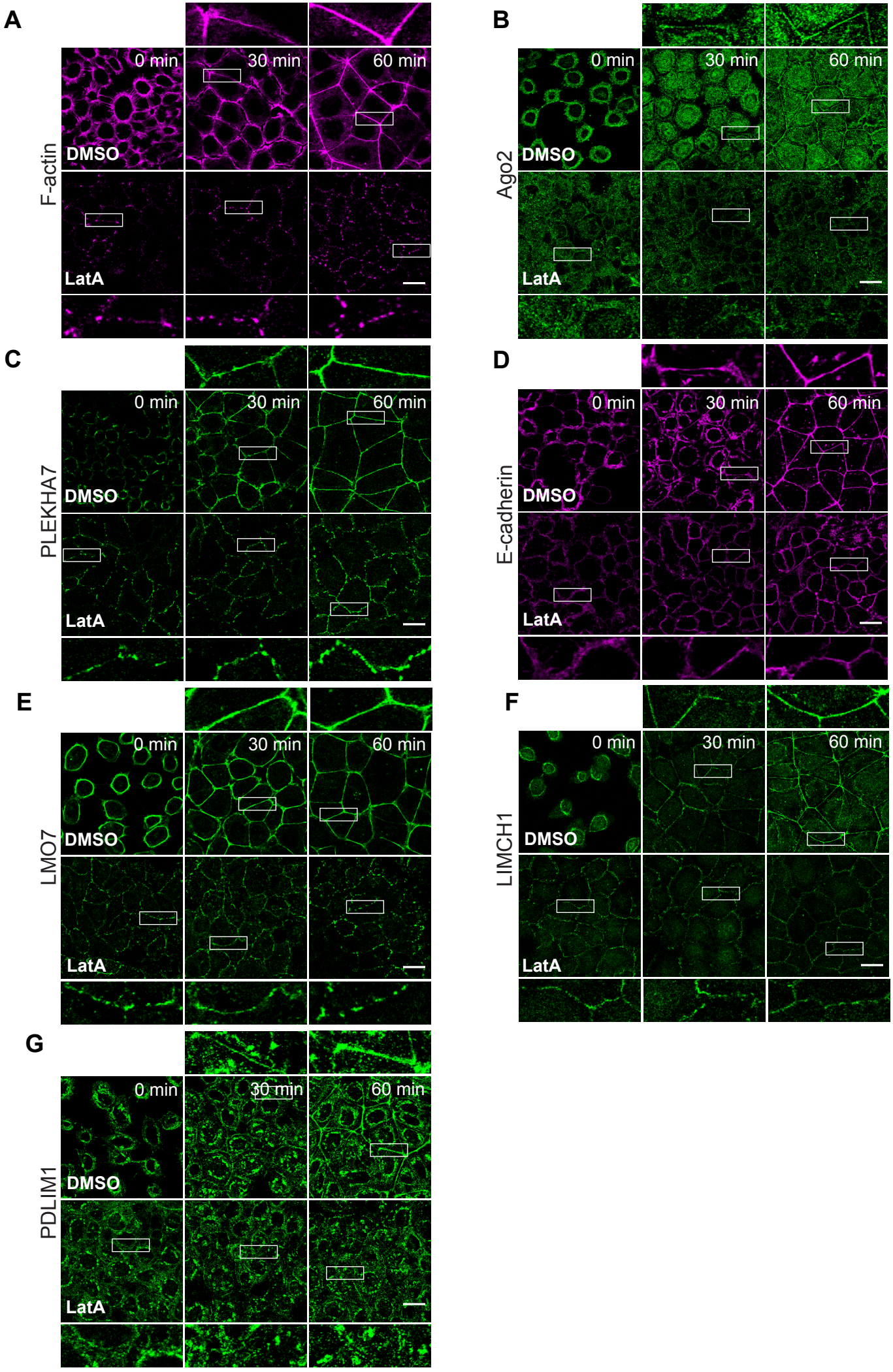
A
F-actin
0 min
30 min
60 min
DMSO
LatA
B
Ago2
0 min
30 min
60 min
DMSO
LatA
C
PLEKHA7
0 min
30 min
60 min
DMSO
LatA
D
E-cadherin
0 min
30 min
60 min
DMSO
LatA
E
LMO7
0 min
30 min
60 min
DMSO
LatA
F
LIMCH1
0 min
30 min
60 min
DMSO
LatA
G
PDLIM1
0 min
30 min
60 min
DMSO
LatA

Fig. 4

Figure 4. Ago2 recruitment to apical adherens junctions is actin-dependent.
(A-G) Immunofluorescence of Caco2 cells fixed at indicated time points throughout a calcium switch assay. Images at 0 min indicate Ca^{2+} depleted cells immediately before Ca^{2+} reintroduction and at 30, 60 min time points are following Ca^{2+} re-addition. Cells were pre-treated and maintained in either DMSO vehicle (control) or 10 µM Latrunculin A (LatA) throughout the calcium switch assay. Insets are marked by white rectangles and are 3X magnification of the original image. Scale bars = 20 µm.

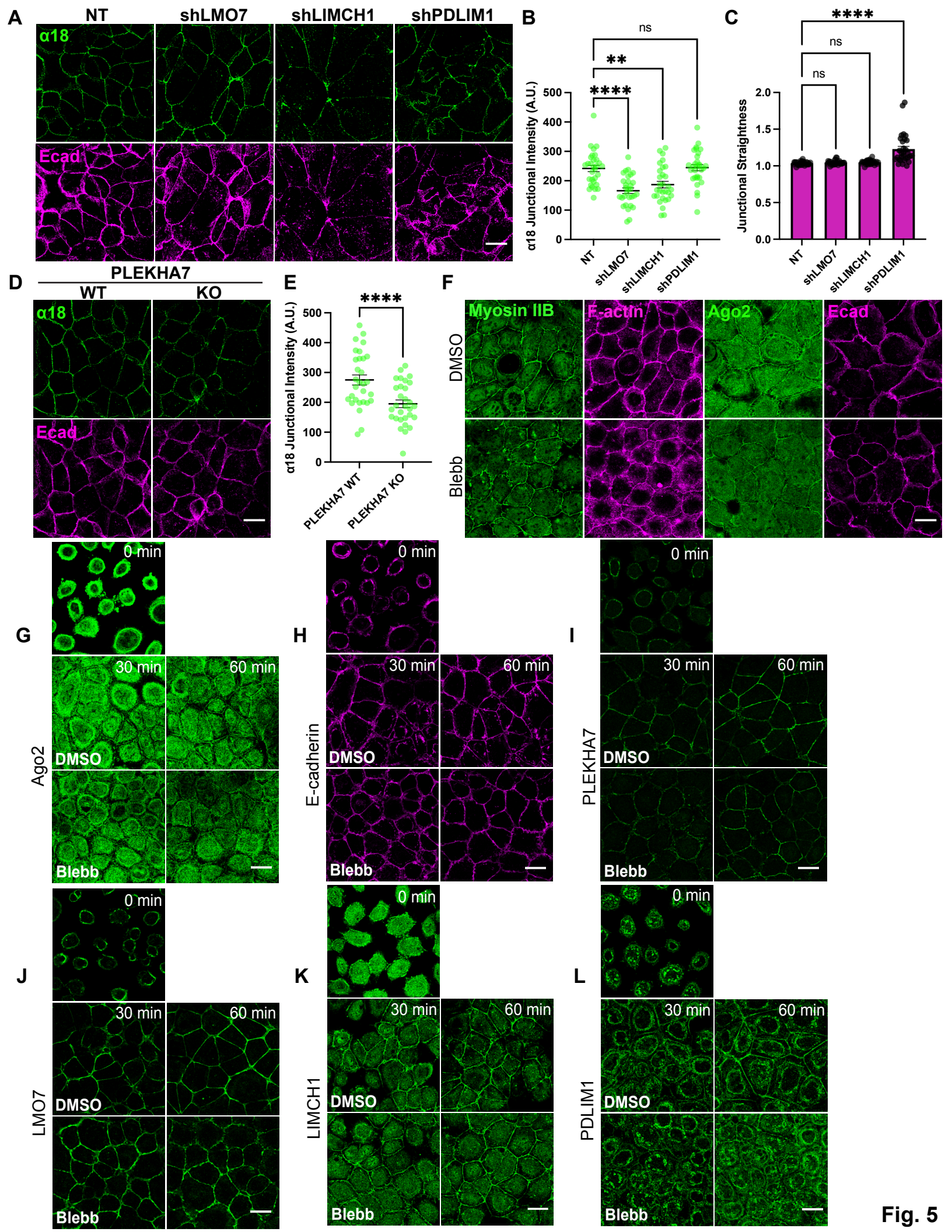
A
NT
shLMO7
shLIMCH1
shPDLIM1
α18
Ecad
B
ns
**
****
α18 Junctional Intensity (A.U.)
500
400
300
200
100
0
NT
shLMO7
shLIMCH1
shPDLIM1
C
****
ns
ns
Junctional Straightness
2.0
1.5
1.0
0.5
0.0
NT
shLMO7
shLIMCH1
shPDLIM1
D
PLEKHA7
WT
KO
α18
Ecad
E
****
α18 Junctional Intensity (A.U.)
500
400
300
200
100
0
PLEKHA7 WT
PLEKHA7 KO
F
Myosin IIB
F-actin
Ago2
Ecad
DMSO
Blebb
G
0 min
30 min
60 min
Ago2
DMSO
Blebb
H
0 min
30 min
60 min
E-cadherin
DMSO
Blebb
I
0 min
30 min
60 min
PLEKHA7
DMSO
Blebb
J
0 min
30 min
60 min
LMO7
DMSO
Blebb
K
0 min
30 min
60 min
LIMCH1
DMSO
Blebb
L
0 min
30 min
60 min
PDLIM1
DMSO
Blebb

Fig. 5

Figure 5. Contractile actin tension at the ZA is disrupted in LMO7, LIMCH1, PDLIM1 knockdown and PLEKHA7 knockout cells and is critical for Ago2 junctional recruitment.
(A-E) Immunofluorescence (IF) using the α18 antibody that recognizes α-catenin upon tension, in control (NT) or LMO7, LIMCH1, and PDLIM1 knockdown (shLMO7, shLIMCH1, shPDLIM1) Caco2 cells and in wild type (WT) or PLEKHA7 knockout (KO) cells, followed by quantification of α18 fluorescence intensity measurements **(B, E)** and quantification of junctional length measurements ("straightness") **(C)**. E-cadherin (Ecad) is used as a co-stain denoting adherens junctions. For quantifying junctional measures in **(B, C, E)**, n= 30 individual junctions for each condition obtained by measuring 10 junctions/field from 3 fields. **(F)** IF of confluent Caco2 cell monolayers, treated with DMSO vehicle or 50 µM Blebbistatin (Blebb) for 3 h. Ecad denotes adherens junctions. **(G-L)** Immunofluorescence of Caco2 cells during a calcium switch assay in which DMSO or Blebbistatin were included in the calcium-containing recovery medium. Cells fixed at 30, 60 min post Ca^{2+} reintroduction were stained for Ago2 **(G)**, E-cadherin **(H)**, PLEKHA7 **(I)**, LMO7 **(J)**, LIMCH1 **(K)**, and PDLIM1 **(L)**. Statistical analyses were performed using one-way ANOVA tests **(B, C)** or unpaired two-way *t* tests **(E)**. Error bars represent mean ± SEM. ****, $P < 0.0001$; ***, $P < 0.001$; **, $P < 0.01$. Scale bars= 20 µm.

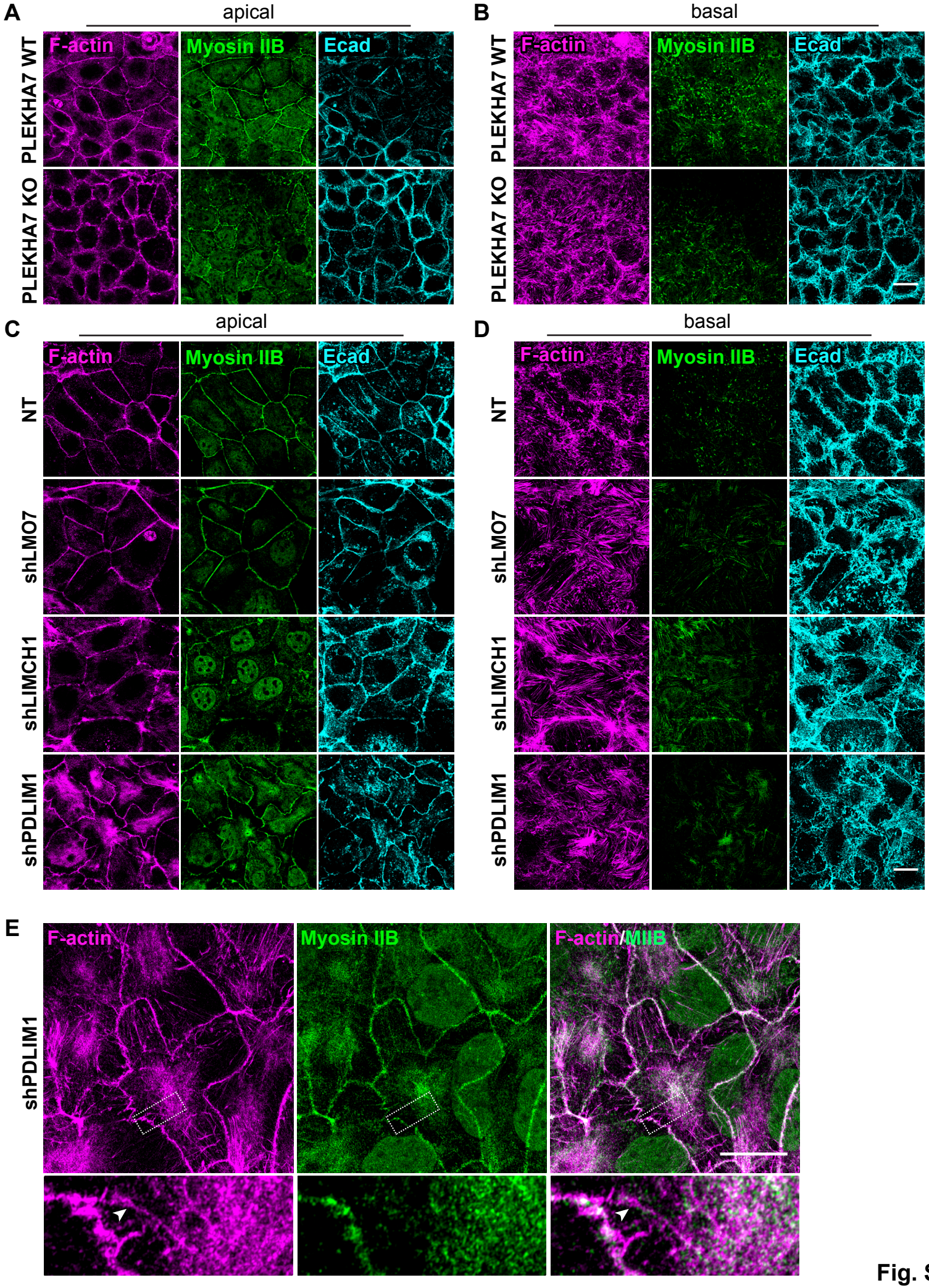
A
apical
F-actin
Myosin IIB
Ecad
PLEKHA7 WT
PLEKHA7 KO
B
basal
F-actin
Myosin IIB
Ecad
PLEKHA7 WT
PLEKHA7 KO
C
apical
F-actin
Myosin IIB
Ecad
NT
shLMO7
shLIMCH1
shPDLIM1
D
basal
F-actin
Myosin IIB
Ecad
NT
shLMO7
shLIMCH1
shPDLIM1
E
F-actin
Myosin IIB
F-actin/MIIB
shPDLIM1

Fig. S1

Figure S1. Actomyosin organization in PLEKHA7 knockout and LMO7, LIMCH1, PDLIM1 knockdown cells. Immunofluorescence (IF) and confocal imaging of **(A, B)** wild type (WT) or PLEKHA7 knockout (KO) Caco2 cells, and (**C,D**) of control (NT) or LMO7, LIMCH1, and PDLIM1 knockdown (shLMO7, shLIMCH1, shPDLIM1) Caco2 cells, accompanying super resolution imaging (see Fig. 3). Representative apical and basal Z-slices are shown. **(E)** Maximum intensity projection of the entire z-plane acquired through super resolution microscopy for the shPDLIM1 field shown in Fig. 3 B. The whole field is shown, as well as the insets included at the bottom of Fig. 3 B. All scale bars= 20 µm.

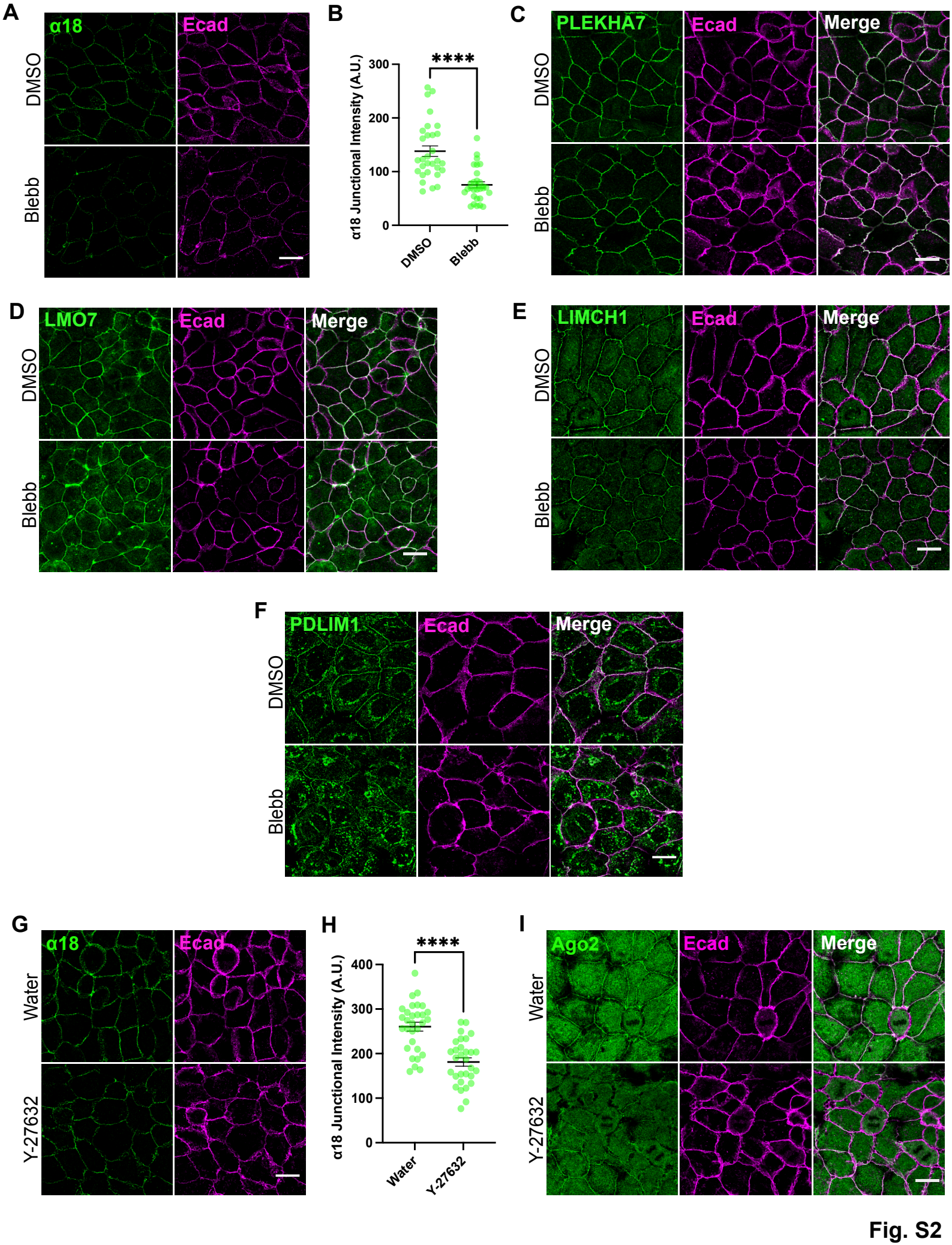
A
α18
Ecad
DMSO
Blebb
B
****
α18 Junctional Intensity (A.U.)
300
200
100
0
DMSO
Blebb
C
PLEKHA7
Ecad
Merge
DMSO
Blebb
D
LMO7
Ecad
Merge
DMSO
Blebb
E
LIMCH1
Ecad
Merge
DMSO
Blebb
F
PDLIM1
Ecad
Merge
DMSO
Blebb
G
α18
Ecad
Water
Y-27632
H
****
α18 Junctional Intensity (A.U.)
400
300
200
100
0
Water
Y-27632
I
Ago2
Ecad
Merge
Water
Y-27632

Fig. S2

Figure S2. Blebbistatin and Y-27632 treatments in confluent Caco2 monolayers disrupt junctional recruitment of Ago2. (A) Immunofluorescence (IF) and **(B)** fluorescence intensity quantification of the α-catenin, α18 antibody in confluent Caco2 cells, treated with DMSO vehicle or 50 µM Blebbistatin (Blebb) for 3 h. For quantification, n= 30 individual junctions/treatment group obtained by measuring 10 borders/field from 3 fields. Statistical analysis was performed using an unpaired two-way *t* test and error bars represent mean ± SEM. ****, $P < 0.0001$. Scale bars= 20 µm. **(C-F)** IF of PLEKHA7 **(C)**, LMO7 **(D)**, or LIMCH1 **(E)** and PDLIM1 **(F)** in confluent Caco2 cells, treated with DMSO vehicle or 50 µM Blebbistatin (Blebb). **(G)** Immunofluorescence (IF) and **(H)** fluorescence intensity quantification of the α-catenin, α18 antibody in confluent Caco2 cells, treated with water vehicle or 20 µM of the ROCK inhibitor Y-27632 for 2 h. For quantification, n= 30 individual junctions/treatment group obtained by measuring 10 borders/field from 3 fields. Statistical analysis was performed using an unpaired two-way *t* test and error bars represent mean ± SEM. ****, $P < 0.0001$. Scale bars= 20 µm. **(I)** IF of Ago2 in confluent Caco2 cells, treated with water vehicle or 20 µM Y-27632. In all cases, E-cadherin (Ecad) is used as a co-stain denoting adherens junctions.

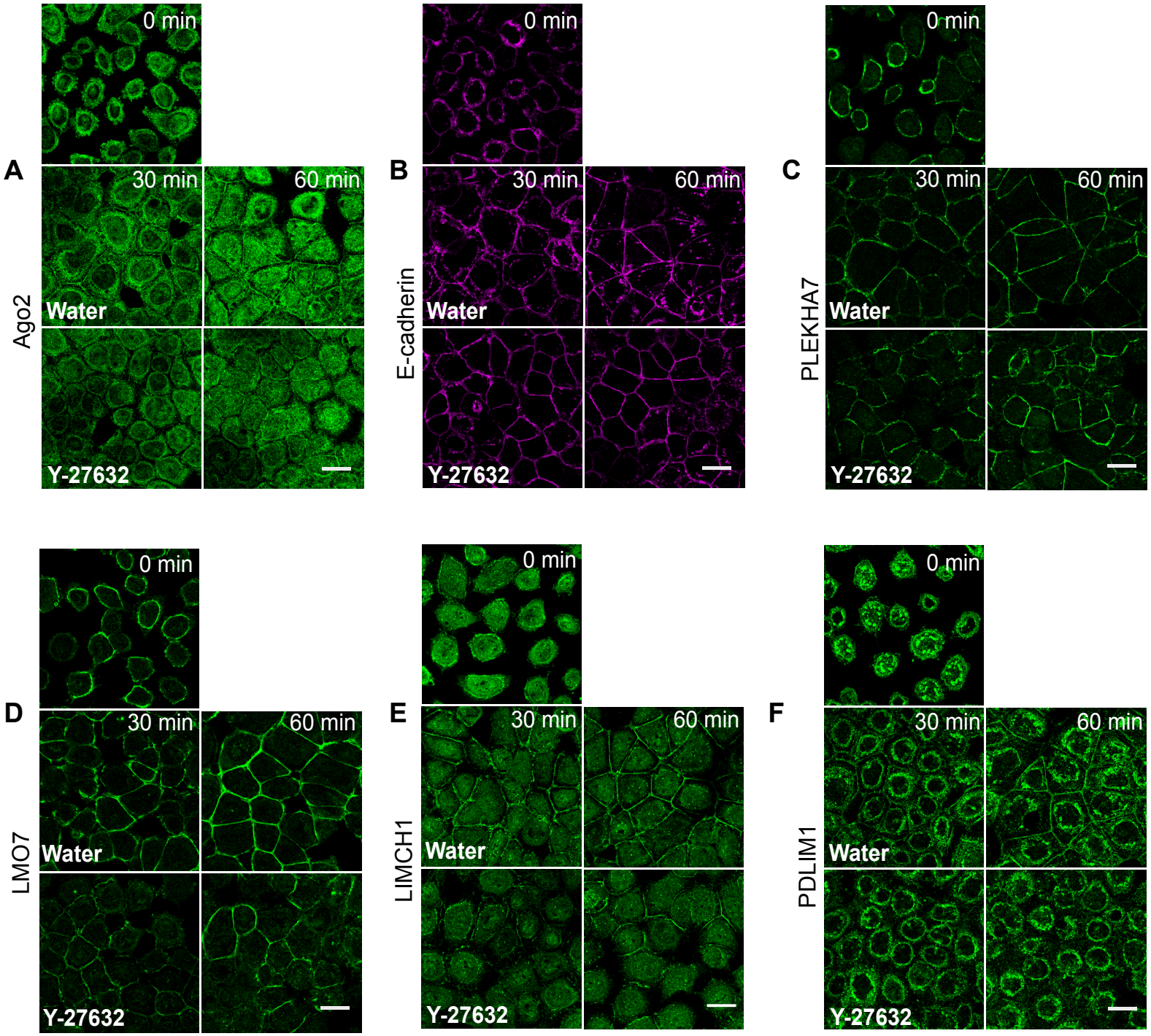

G

Homo sapiens chromosome 11, GRCh38.p13 Primary Assembly
REGION: complement (16777297..17014423)
gene="PLEKHA7"

Caco2_16P allele #1: -127 bp

```
16855723 ttgggttgttctaaggcccaacaaccgattcctacctggaactgatcttactgcacttcctactctatagctcggcttttactcactggaatcccctgtctcctcacaggccgaatccacatatgtcgaagcaagacagaaaccaaagac 16855873
16855874 cgtccagcatggtcagtgaaacatccacggctgggaccgcctccaccctggaggccaagcctggacccaaggtgagctcctggccacttgttccttccttcccttctttatattttgccaagcccctttgtaaccagaagtccatttga 16856023
```

Caco2_16P allele #2: -127 bp

```
16855723 ttgggttgttctaaggcccaacaaccgattcctacctggaactgatcttactgcacttcctactctatagctcggcttttactcactggaatcccctgtctcctcacaggccgaatccacatatgtcgaagcaagacagaaaccaaagac 16855873
16855874 cgtccagcatggtcagtgaaacatccacggctgggaccgcctccaccctggaggccaagcctggacccaaggtgagctcctggccacttgttccttccttcccttctttatattttgccaagcccctttgtaaccagaagtccatttga 16856023
```

Caco2_16P allele #3: -127 bp

```
16855723 ttgggttgttctaaggcccaacaaccgattcctacctggaactgatcttactgcacttcctactctatagctcggcttttactcactggaatcccctgtctcctcacaggccgaatccacatatgtcgaagcaagacagaaaccaaagac 16855873
16855874 cgtccagcatggtcagtgaaacatccacggctgggaccgcctccaccctggaggccaagcctggacccaaggtgagctcctggccacttgttccttccttcccttctttatattttgccaagcccctttgtaaccagaagtccatttga 16856023
```

gRNA

Fig. S3

Figure S3. Y-27632 treatment during recovery following calcium depletion results in loss of junctional Ago2. (A-F) Immunofluorescence of a calcium switch assay in which water vehicle or 30 µM Y-27632 were included in the calcium-containing recovery medium. Cells fixed immediately before Ca^{2+} reintroduction (0 min) or 30, 60 min post Ca^{2+} addition were stained for Ago2 **(A)**, E-cadherin **(B)**, PLEKHA7 **(C)**, LMO7 **(D)**, LIMCH1 **(E)**, and PDLIM1 **(F)**. Scale bars= 20 µm. **(G)** PLEKHA7 CRISPR/Cas9 knockout validation. Sequencing of the genomic region of PLEKHA7 that was targeted by CRISPR/Cas9 in the PLEKHA7 knockout Caco2 cells (clone 16P) used in the present study. The guide RNA (gRNA) sequence used is underlined. The sequenced regions were aligned against the human genome GRCh38.p13 Primary Assembly. The deleted regions detected in PLEKHA7 alleles are highlighted (Caco2 cells exhibit polyploidy).